
This is the **accepted version** of the journal article:

Urciuoli, Alessandro; Zanolli, Clément; Alméjida, Sergio; [et al.]. «Reassessment of the phylogenetic relationships of the late Miocene apes Hispanopithecus and Rudapithecus based on vestibular morphology». Proceedings of the National Academy of Sciences of the United States of America, Vol. 118, Issue 5 (January 2021), art. e2015215118. DOI 10.1073/pnas.2015215118

This version is available at <https://ddd.uab.cat/record/258412>

under the terms of the  ^{IN} COPYRIGHT license

1 BIOLOGICAL SCIENCES: Anthropology

2

3 **Reassessment of the phylogenetic relationships of the late Miocene apes**

4 ***Hispanopithecus* and *Rudapithecus* based on vestibular morphology**

5

6 Alessandro Urciuoli^{a,*}, Clément Zanolli^b, Sergio Almécija^{c,d,a}, Amélie Beaudet^{e,f}, Jean

7 Dumoncel^g, Naoki Morimoto^h, Masato Nakatsukasa^h, Salvador Moyà-Solà^{a,i,j}, David

8 R. Begun^k, David M. Alba^{a,*}

9

10 ^aInstitut Català de Paleontologia Miquel Crusafont, Universitat Autònoma de

11 Barcelona, Edifici ICTA-ICP, c/ Columnes s/n, Campus de la UAB, 08193

12 Cerdanyola del Vallès, Barcelona, Spain; ^b*Univ. Bordeaux, CNRS, MCC, PACEA,*

13 *UMR 5199, F-33600 Pessac, France;* ^cDivision of Anthropology, American Museum

14 of Natural History, Central Park West at 79th Street, New York, NY 10024, USA;

15 ^dNew York Consortium in Evolutionary Primatology, New York, USA; ^eSchool of

16 Geography, Archaeology and Environmental Studies, University of the

17 Witwatersrand, Private Bag 3, Johannesburg, WITS 2050, South Africa; ^fDepartment

18 of Anatomy, University of Pretoria, PO Box 2034, Pretoria, 0001, South Africa;

19 ^gLaboratoire AMIS, UMR 5288 CNRS, Université de Toulouse, Allées Jules Guesde

20 37, 31073, Toulouse, France; ^hLaboratory of Physical Anthropology, Graduate

21 School of Science, Kyoto University, Kyoto, 606 8502, Japan; ⁱInstitució Catalana de

22 Recerca i Estudis Avançats (ICREA), Passeig de Lluís Companys 23, 08010

23 Barcelona, Spain; ^jUnitat d'Antropologia (Departament de Biologia Animal, Biologia

24 Vegetal i Ecologia), Universitat Autònoma de Barcelona, Campus de la UAB s/n,

25 08193 Cerdanyola del Vallès, Barcelona, Spain; ^kDepartment of Anthropology,

26 University of Toronto, Toronto, ON M5S 2S2, Canada

27

28 *To whom correspondence should be addressed:

29

30 Alessandro Urciuoli

31 Postal address: Institut Català de Paleontologia Miquel Crusafont, Universitat
32 Autònoma de Barcelona, Edifici ICTA-ICP, c/ Columnes s/n, Campus de la UAB,
33 08193 Cerdanyola del Vallès, Barcelona, Spain

34 Phone: +34 622112509

35 Email: alessandro.urciuoli@icp.cat

36

37 David M. Alba

38 Postal address: Institut Català de Paleontologia Miquel Crusafont, Universitat
39 Autònoma de Barcelona, Edifici ICTA-ICP, c/ Columnes s/n, Campus de la UAB,
40 08193 Cerdanyola del Vallès, Barcelona, Spain

41 Phone: +34 935868604

42 Email: david.alba@icp.cat

43

44 **Keywords:** inner ear, semicircular canals, evolution, fossil apes, Hominidae.

45

46 ORCID:

47 Alessandro Urciuoli: 0000-0002-6265-8962

48 Clément Zanolli: 0000-0002-5617-1613

49 Sergio Almécija: 0000-0003-1373-1497

50 Amélie Beaudet: 0000-0002-9363-5966

51 Jean Dumoncel: 0000-0003-0789-7458

52 Naoki Morimoto: 0000-0002-8367-4777

53 Masato Nakatsukasa: 0000-0002-6897-8027

54 Salvador Moyà-Solà: 0000-0001-8506-1061

55 David R. Begun: 0000-0001-8916-6442

56 David M. Alba: 0000-0002-8886-5580

57

58

59 **Abstract**

60 **Late Miocene great apes are key to reconstructing the ancestral morphotype**
61 **from which earliest hominins evolved. Despite consensus that the late**
62 **Miocene dryopith great apes *Hispanopithecus laietanus* (Spain) and**
63 ***Rudapithecus hungaricus* (Hungary) are closely related (Hominidae), ongoing**
64 **debate on their phylogenetic relationships with extant apes (stem hominids,**
65 **hominines, or pongines) complicates our understanding of great ape and**
66 **human evolution. To clarify this question, we rely on the morphology of the**
67 **inner ear semicircular canals, which has been shown to be phylogenetically**
68 **informative. Based on microcomputed tomography scans, we describe the**
69 **vestibular morphology of *Hispanopithecus* and *Rudapithecus*, and compare**
70 **them with extant hominoids using landmark-free deformation-based 3D**
71 **geometric morphometric analyses. We also provide critical evidence about the**
72 **evolutionary patterns of the vestibular apparatus in living and fossil hominoids**
73 **under different phylogenetic assumptions for dryopiths. Our results are**
74 **consistent with the distinction of *Rudapithecus* and *Hispanopithecus* at the**
75 **genus rank, and further support their allocation to the Hominidae based on**
76 **their derived semicircular canal volumetric proportions. Compared with extant**
77 **hominids, the vestibular morphology of *Hispanopithecus* and *Rudapithecus***
78 **most closely resembles that of African apes, and differs from the derived**
79 **condition of orangutans. However, the vestibular morphologies reconstructed**
80 **for the last common ancestors of dryopiths, crown hominines, and crown**
81 **hominids are very similar, indicating that hominines are plesiomorphic in this**
82 **regard. Therefore, our results do not conclusively favor a hominine or stem**
83 **hominid status for the investigated dryopiths.**

84

85 **Significance**

86 Reconstructing the phylogenetic relationships of extinct apes is challenging due to
87 their fragmentary fossil record and the recurrent independent evolution of
88 morphological features. Given the relevance of the phylogenetic signal of the bony
89 labyrinth, here we assess the phylogenetic affinities of the late Miocene great apes
90 *Hispanopithecus* and *Rudapithecus* by studying their inner ear morphology. Our
91 results are consistent with the distinct generic status of these dryopiths, which further
92 differ from the derived condition of orangutans and most closely resemble African
93 apes. However, the latter appear largely primitive (similar to the last common
94 ancestor of great apes and humans), hence our results do not conclusively favor a
95 closer relationship with African apes as opposed to great apes as a whole.

96

97

98 Hominoids (apes and humans) originated in Africa during the Oligocene (1) but
99 subsequently dispersed into Eurasia, giving rise to an impressive radiation during the
100 middle and late Miocene (2-3). Thus, while extant hominoids include only two
101 moderately diverse families—hylobatids (gibbons and siamangs) and hominids
102 (great apes and humans)—the panoply of extinct genera recorded during the
103 Miocene still defies classification into a coherent systematic scheme. Other than the
104 late Miocene *Oreopithecus*—which might be a late occurring stem hominoid (4, 5) —
105 there is consensus that most Eurasian large-bodied hominoids are members of the
106 great-ape-and-human clade (Hominidae) (2, 3, 6). While most Asian extinct great
107 apes such as *Sivapithecus* are considered to be more closely related to the
108 orangutan clade (Ponginae) than to African apes and humans (Homininae) (2, 6-8),
109 the phylogenetic affinities of European *Dryopithecus* and allied forms have long been
110 debated. Until a decade ago, several species of European apes from the middle and
111 late Miocene were included within this genus (9-16). However, discoveries at the
112 middle Miocene composite section of Abocador de Can Mata (6, 17-20) prompted
113 the recognition that the late Miocene species belong to one or more different genera
114 distinct from/other than *Dryopithecus* (2-3, 6, 7, 18, 21-26): *Hispanopithecus* from
115 Spain, and *Rudapithecus* from Hungary, the latter formerly considered a subgenus of
116 the former by some authors (6, 18, 22).

117 Together with *Dryopithecus* and other middle to late Miocene taxa (17, 19, 27),
118 *Hispanopithecus* and *Rudapithecus* are currently classified in a subfamily
119 (Dryopithecinae) (6, 20, 26) or tribe (Dryopithecini) (3, 7, 21) of their own, distinct
120 from pongines. Both taxa possess a hominid-like cranial morphology (6, 11-13, 21,
121 25, 29-30), as shown by the high zygomatic root, reduced midfacial prognathism,
122 lack of subarcuate fossa, deep glenoid fossa, and prominent entoglenoid process.

123 However, there is no consensus regarding the phylogenetic position of this group—
124 being either considered stem hominids (6, 19, 28), stem hominines (2-3, 14, 16, 25),
125 or even pongines (10, 29-30) —which may be informally referred to as ‘dryopiths’.
126 Resolving the phylogenetic position of dryopiths has important implications for the
127 evolution of the great ape and human clade, since their purported hominine status
128 has led to paleobiogeographic scenarios favoring a European origin and subsequent
129 back-to-Africa dispersal for the African and human clade (2-3, 15, 24-25).
130 Disagreements and uncertainties about the phylogenetic position of extinct apes are
131 persistent, and stem from a combination of factors, including the incomplete and
132 fragmentary hominoid fossil record, the decimated current diversity of the group, and
133 pervasive homoplasy coupled with mosaic evolution (6, 23, 31-35).

134 The morphology of the semicircular canals (SCs), which partly constitute the inner
135 ear’s bony labyrinth, has been classically related to locomotion (36-42). However,
136 several studies have highlighted the possibility of inferring phylogenetic relatedness
137 based on this portion of the inner ear morphology (43-47) Recently, it has been
138 shown that this anatomical structure also embeds a strong phylogenetic signal
139 among catarrhine primates by means of 3D geometric morphometric (3DGM)
140 analyses (5, 47-49), thus being potentially useful to test phylogenetic hypotheses for
141 extinct hominoids. Previous studies relied on the SC radius of *Rudapithecus*
142 *hungaricus* and *Hispanopithecus laietanus* to infer slow and deliberate arboreal
143 locomotion for these species (41). However, recent analyses raised doubts about the
144 reliability of locomotor behavior predictions based on SC radius only (50-51). In
145 contrast, here we rely on μ CT scans of the same specimens and a deformation-
146 based (landmark-free) 3DGM approach to assess their closest affinities in SC
147 morphology with extant hominoids and interpret them from an evolutionary viewpoint.

148 First, we describe the fossil remains and qualitatively compare them with extant
149 hominoids. Second, we assess if the volumetric proportions of their SCs more
150 closely resemble those of hominids than those of other anthropoids. Third, we
151 quantitatively evaluate changes in SC and vestibule morphology by means of a
152 between-group principal component analysis (bgPCA) applied to a sample of extant
153 and extinct hominoids. The affinities of the investigated fossil taxa are further
154 assessed by means of cluster analyses and group membership probabilities based
155 bgPCA results. Finally, we reconstruct the evolutionary history of the hominoid SCs
156 using a phylomorphospace approach (including reconstructed ancestral
157 morphotypes) under various phylogenetic assumptions for dryopiths.

158

159 **Results**

160 **Descriptions and comparisons.** Three-dimensional renderings of the vestibular
161 apparatus of fossil and extant hominoids investigated here are illustrated in the
162 Figure 1a-m. The vestibular apparatus of *R. hungaricus* is well preserved in the three
163 available specimens (Fig. 1a-c). As in extant hominids, the SCs are stout—although
164 less so than in orangutans (Fig. 1j), most humans (Fig. 1m) and gorillas (Fig. 1k)—
165 and the vestibule is large relative to the volume occupied by SCs. The anterior and
166 posterior canals are large and similar in size (Fig. 1a,b). The anterior canal is slightly
167 vertically compressed, as in extant hominoids and the fossil apes *Nyanzapithecus*
168 *alesi* (4) and *Nacholapithecus kerioi* (Fig. 1f), and somewhat larger in RUD 77 than
169 in RUD 200. The anterior canal is somewhat anterosuperiorly projecting, albeit much
170 less so than in *Pongo* (Fig. 1j) and *Oreopithecus* (Fig. 1e). The lateral and posterior
171 canals are slightly different between the two individuals. In RUD 77, the lateral canal
172 is noticeably smaller than the other SCs (Fig. 1a,b), slightly compressed horizontally,

173 and slenderer than in RUD 200. The lateral canal of RUD 200 is stout and large,
174 almost reaching the size of the vertical SCs (similar to the condition in African apes,
175 yet smaller than in gorillas; Fig. 1c), and its slender portion connects with the
176 vestibule somewhat more inferiorly than in RUD 77. The junction of the slender
177 portion of the lateral canal and the ampulla further differs between the two
178 individuals, as it protrudes anteriorly in RUD 200, while it is posterolaterally oriented
179 in RUD 77. In both individuals, the ampullary portion bends superiorly and the
180 slender segment between the connection with the vestibule and the posterolateral tip
181 of the lateral canal is straight, as in *Hoolock* (Fig. 1g) and in most hominids (Fig. 1j-
182 m)—except for some *Gorilla* and *Pan* specimens that show some curvature.
183 However, this section of the canal is more laterally oriented in RUD 77, while it is
184 almost parallel to the posterior canal in RUD 200. The posterior canal is elongated
185 posterolaterally in RUD 77, as in gorillas (Fig. 1k) and some humans (Fig. 1m), while
186 it is slightly more rounded in RUD 200 (Fig. 1c). In both RUD 77 and RUD 200, the
187 posterior and lateral canals approximately define a right angle (slightly more obtuse
188 in RUD 77) and the trajectory of the lateral canal does not intersect the plane
189 identified by the posterior canal. The common crus (CC) is short and slender, with
190 the slender portions of the anterior and posterior canals almost forming right angle at
191 the CC apex. The SCs are almost coplanar, with a slight amount of torsion in the
192 upper portion of the anterior one (the tip slightly bending medially), in the medial-
193 most part of the posterior one (displaced anteriorly), and in the tip of the lateral canal
194 (pointing inferiorly).

195 The vestibular apparatus of *H. laietanus* (Fig. 1d) differs from that of *Rudapithecus*
196 (especially RUD 77; Fig. 1a,b) by being more voluminous and displaying more
197 equally developed SCs. The larger volume is particularly appreciable on the

198 vestibular recesses (which are more voluminous than the SCs, as in orangutans; Fig.
199 1j) and in the much more inflated ampullae. The anterior canal is more vertically
200 compressed than in *Rudapithecus*, showing an almost rectangular shape. This canal
201 is also much slenderer than in orangutans (Fig. 1j) and gorillas (Fig. 1k), most
202 closely resembling chimpanzees (Fig. 1l). The lateral canal is stouter than the others,
203 especially in the ampullary portion. Its posterolateral-most tip slightly bends inferiorly,
204 resulting in a moderate torsion of the canal. The slender segment between the
205 connection with the vestibule and the posterolateral tip of the lateral canal is straight,
206 as in *Rudapithecus* (Fig. 1a-c), *Hoolock* (Fig. 1g) and most hominids (Fig. 1j-m), and
207 laterally oriented, as in *Pongo* (Fig. 1j), some humans (Fig. 1m) and RUD 77 (Fig.
208 1a-b). The ampullary portion of the lateral canal is bent superiorly, as in
209 *Rudapithecus* (Fig. 1a-c) and extant hominoids (Fig. 1g-m). However, unlike extant
210 great apes (Fig. 1j-l) and *Rudapithecus* (Fig. 1a-c), the portion between the ampulla
211 and the tip of the lateral canal is inflated. The posterior canal is small and rounded,
212 with a large ampulla. The CC is longer than in *Rudapithecus* (Fig. 1a-c) and in most
213 extant great apes (with *Pongo* showing the shortest), yet more inflated (even if much
214 less so than in orangutans; Fig. 1j), and the CC apex forms an obtuse angle. As in
215 *Rudapithecus* and extant hominids, the planes identified by the lateral and posterior
216 canals form a right angle and their trajectories do not intersect.

217

218 **Volumetric proportions.** Allometric regressions of SC volume vs. length were
219 performed separately for hominoids and the rest of anthropoids included in the
220 sample (Fig. 2a; measurements for the dryopiths are given in Supplementary Table
221 1) because it has been previously shown that the former display an allometric grade
222 shift toward relatively higher volumes at a comparable length once size-scaling

223 effects have been taken into account (5), with only minimal overlap. *Hispanopithecus*
224 falls above the hominid regression line, while *Rudapithecus* is situated more (RUD
225 77) or less (RUD 200) below the line, close to *Nacholapithecus*, but in all cases
226 within the range of extant hominids and well above the regression line of other
227 anthropoids (Fig. 2a). Gorillas are variable in this regard, while humans and
228 orangutans display stouter proportions than chimpanzees and bonobos (Fig. 2b).
229 The SCs of *Hispanopithecus* appear intermediate between these aforementioned
230 taxa (closer to humans and orangutans), while those of *Rudapithecus*, *Oreopithecus*,
231 and *Nacholapithecus* are slenderer and more comparable to those of chimpanzees
232 and bonobos. Overall, given their range of variation, all the extinct apes analyzed
233 here display extant hominid-like volumetric proportions of the vestibular apparatus.

234

235 **Shape analysis.** The bgPCA (Fig. 3), based on the deformation fields computed for
236 the hominoid sample, allows us to discriminate extant hominoid species, as shown
237 by classification results (99% of correctly classified individuals before and after cross
238 validation). These results closely resemble those computed using a cross-validated
239 bgPCA (Supplementary Fig.1). We also recover very significant group mean
240 differences ($p < 0.001$) for the raw shape data (Supplementary Table 2), confirming
241 that group structure does not artifactually result from the bgPCA (52). Indeed, group
242 differences account for a substantial amount of variance (R^2) in the raw shape data,
243 indicating that group separation is not spurious (52), although intergroup variance is
244 increased to a similar extent by the standard bgPCA space and the cross-validated
245 bgPCA (Supplementary Table 2).

246 bgPC1 (40.7% of the total variance) pulls apart hominids (mostly positive values)
247 from hylobatids (negative values), with no overlap. Positive values along this axis

248 indicate short and bulgy SCs, together with a right angle between the anterior and
249 posterior semicircular canals. Orangutans and humans display the most extreme
250 condition due to the stoutness of their SCs. Chimpanzees, bonobos, and gorillas
251 show a broad range of variation, with some individuals close to the origin due to their
252 somewhat slenderer SCs (albeit less so than in hylobatids, which display negative
253 values), and others overlapping with *Pongo* and *Homo*. Along bgPC1,
254 *Hispanopithecus* overlaps with australopiths, extant great apes, and humans, while
255 the *Rudapithecus* specimens fall within the African great ape range. Both RUD 77
256 and RUD 200 closely approach the origin, with the latter showing slightly more
257 positive values. *Oreopithecus* and *Nacholapithecus* are found on moderate negative
258 values, within the lower range of *Pan* and *Gorilla*, due to their quite slender SCs
259 (albeit clearly stouter than in hylobatids).

260 The patterns of shape variation captured by bgPC2 (33.4% of total variance; Fig.
261 3a) reflect changes in the shape of three canals as well as their relative proportions.
262 In particular, bgPC2 clearly discriminates *Homo* (with most negative values) from the
263 rest of the sample, due to the presence in the former of a large and rounded
264 (sometimes even slightly superiorly elongated) anterior canal, a posterolaterally
265 displaced inferior portion of the posterior canal, and a small, fairly anterolaterally
266 elongated lateral canal, whose slender portion connects to the vestibule more
267 superiorly and anterolaterally than in apes. The latter fall on intermediate and
268 positive values, with hylobatids considerably overlapping with *Pan* spp. (Fig. 3a). To
269 a large extent, this is due to their anterior canal shape, which appears intermediate
270 between the rounded morphology of humans and the marked vertical compression of
271 *Pongo* and *Gorilla* (the latter taxa occupying more positive values with only very
272 slight overlap with *Pan* and hylobatids). Both *Rudapithecus* and *Hispanopithecus*,

273 like *Oreopithecus* and *Nacholapithecus*, show intermediate values along this axis,
274 overlapping with hylobatids and *Pan* spp. (as well as the *Australopithecus* specimen
275 StW 573), but not with *Pongo* and *Gorilla*. Conversely, the other australopith (StW
276 578) more closely approaches humans due to its larger vertical SCs.

277 bgPC3 (11.4% of variance; Fig. 3b) is driven by the shape of the anterior canal, its
278 relative size relative compared with that of the lateral one, the length of the CC, and
279 the amount of torsion of the lateral canal. Thus, negative values reflect a large and
280 anterosuperiorly projecting anterior canal, coupled with a small lateral one, and a
281 short CC. This axis discriminates *Pongo* (most negative values) from the rest of the
282 sample, only minimally overlapping with some *Hylobates*. One individual of
283 *Rudapithecus* (RUD 77) and *Oreopithecus* overlap with the range of orangutans due
284 to their anterosuperiorly projecting anterior canal (albeit less so in RUD 77), short
285 CC, and markedly small lateral canal. A similar morphology of the anterior canal is
286 also found in some *Hylobates* and in one of the *Australopithecus* specimens (StW
287 573), resulting in moderately negative scores. *Hispanopithecus* and the other
288 individual of *Rudapithecus* (RUD 200) fall at the negative end of the gorilla and
289 human variation, due to their intermediate anterior canal morphology, longer CC (yet
290 less so than in most *Pan* and *Gorilla* individuals), and a larger lateral canal.
291 *Nacholapithecus* and the other australopith specimen (StW 578) fall among
292 moderate positive values, overlapping with gorillas, chimpanzees, bonobos, humans,
293 and hylobatids, due to their long CC and more vertically aligned (i.e., superiorly
294 directed) connection of the anterior canal with the CC.

295 When the inspected bgPCs are considered simultaneously to compute posterior
296 probabilities of group membership (Table 1), the *Rudapithecus* RUD 77 individual
297 occupies a position in the morphospace that does not fit well with most extant

298 hominoid genera ($p < 0.05$), rather approaching the position of *Nacholapithecus* and
299 *Oreopithecus* in the morphospace (Table 2). Conversely, RUD 200 shows
300 considerable similarities with *Pan* ($p = 0.549$) and *Nacholapithecus*. The three
301 *Rudapithecus* specimens fall closer to one another than either approaches the single
302 specimen of *Hispanopithecus* (Table 2), which is also more distant than
303 *Nacholapithecus* from all the considered specimens (Table 2). *Hispanopithecus*
304 mostly differs along bgPC1, sharing similarities in the volumetric proportions of the
305 SCs and in the vertically compressed anterior canal morphology with
306 *Australopithecus* individual StW 573 (Table 2). IPS18000 marginally differs from *Pan*
307 ($p = 0.053$) and is clearly an outlier compared to the remaining extant genera.

308 The cluster analyses based on the significant bgPCs (Fig. 4a) and raw shape data
309 (Fig. 4b) further support the aforementioned results, since *Rudapithecus* and
310 *Hispanopithecus* do not cluster with one another and show affinities with different
311 taxa. In particular, the cluster based on the bgPCA results (Fig. 4a) indicates that
312 *Rudapithecus* is most similar to both *Pan* and *Nacholapithecus*, while
313 *Hispanopithecus* approaches hominins. This is further supported by the raw shape
314 data cluster (Fig. 4b), which mainly differs by recovering a great ape cluster.

315

316 **Phylomorphospace and reconstruction of ancestral morphologies.** The shape
317 data, as captured by the bgPCA performed on the extant hominoid sample,
318 approaches the Brownian motion (BM) model of evolution, as supported by the
319 phylogenetic signal computed for the bgPCs ($K_{\text{mult}}=0.864$, $p=0.019$) and for the raw
320 data (i.e., the deformation fields; $K_{\text{mult}}=0.863$, $p=0.017$). We used phylogenetically
321 informed techniques on the shape data to visualize the direction and magnitude of
322 vestibular shape change during hominoid evolution as well as to depict the internal

323 nodes of the phylogeny—i.e., the inferred vestibular morphology of the last common
324 ancestors (LCAs) of major groups—as reconstructed by maximum likelihood. The
325 results are very similar irrespective of the precise phylogenetic placement of
326 dryopiths as stem hominines (Fig. 5; Supplementary Fig. 2b), stem hominids
327 (Supplementary Fig. 3a, c; Supplementary Fig. 2a), or stem pongines
328 (Supplementary Fig. 3b, d; Supplementary Fig. 2c). The crown hominoid LCA (Figs.
329 5, 6a) is reconstructed as possessing evenly-sized and moderately inflated SCs, a
330 moderately long and not inflated CC, a fairly vertically compressed, yet not
331 anterosuperiorly projecting, anterior canal, an almost rounded posterior canal, an
332 obtuse angle between the planes identified by the anterior and posterior canals
333 (close to the right angle), and a right angle among the SCs merging at the CC apex
334 (Fig. 6a). Irrespective of the phylogenetic assumptions for dryopiths, the
335 reconstructed LCA for crown hominoids is closer to hominids (especially
336 *Nacholapithecus*, *Rudapithecus* and, among extant taxa, *Pan*) than to hylobatids
337 (Fig. 5), in terms of their intermediate volumetric proportions, contrasting with the
338 markedly slenderer SCs of gibbons and siamangs. In turn, the LCAs of crown
339 hominines and dryopiths (*Rudapithecus* + *Hispanopithecus*) closely resemble one
340 another irrespective of the underlying phylogenetic assumptions for the fossil species
341 (Fig. 5, Supplementary Fig. 3), being extant-hominid-like in volumetric proportions
342 but otherwise showing a more plesiomorphic morphology in the evenly sized and
343 fairly rounded SCs.

344 The inferred LCA of crown hominids, in particular, closely resembles that of crown
345 hominoids, except for the stouter volumetric proportions, more derived toward the
346 extant hominid condition (Figs. 5, 6b). It displays equally-sized SCs, an obtuse to
347 right angle in the apex of a moderately long CC, and a slightly laterally elongated

348 posterior canal (Fig. 6b). Orangutans appear derived from the LCA by displaying
349 more inflated SCs (especially the anterior one, Figs. 1j, 6b), further diverging in the
350 opposite direction from African great apes and humans because its short and
351 extremely stout CC, as well as its anterosuperiorly projecting anterior canal and
352 marked torsion of the lateral canal (Fig. 5b). The LCA of hominines (Fig. 6c) appears
353 somewhat more derived than the LCAs of hominoids and hominids for both
354 volumetric proportions and SC shape. It displays moderately stout SCs and
355 medium/large vestibular recesses, equally developed SCs (with a slightly smaller
356 lateral one), a vertically compressed anterior canal (more so than in any other LCA),
357 a slightly laterally projecting posterior canal, and a long CC with an obtuse angle in
358 its apex (Fig. 6c). *Homo* and *Gorilla* would have evolved in opposite directions from
359 this ancestral morphology in terms of SC relative size, with humans showing the
360 largest vertical canals (Figs. 1m, 5a) and gorillas displaying a larger lateral canal
361 (Figs. 1k, 5a). Chimpanzees and bonobos, due to their equally sized SCs and fairly
362 elongated CC (Figs. 1l, 5a), are closer to the hominine LCA morphology, while
363 *Australopithecus* appears derived toward the human condition, due to the moderate
364 increase in the size of the anterior and posterior canals (Fig 5). The reconstructed
365 morphotype for the LCA of the investigated dryopiths (Fig. 6d) closely resembles
366 those of hominines and hominids by displaying moderately stout and evenly-sized
367 SCs (with a slightly smaller lateral one), an obtuse angle at the CC apex, and a not
368 anterosuperiorly projecting anterior canal, differing from the hominid LCA by the
369 somewhat less vertically compressed anterior canal (Fig. 6b,d).

370 *Hispanopithecus* and *Rudapithecus* appear to have diverged in opposite
371 directions from their LCA (Fig. 5). The former seems derived in the volumetric
372 proportions (similarly to, *Pongo*, *Australopithecus*, and *Homo*), whereas the

373 *Rudapithecus* condition in this regard is very similar to that of *Pan* as well as the
374 reconstructed hominid LCA, and (to a lesser extent) to those of *Nacholapithecus* and
375 *Oreopithecus* (Figs. 5, 6b). Likewise, the fairly short CC and a somewhat
376 anterosuperiorly projecting anterior canal found in *Rudapithecus* (less so than in
377 orangutans and *Oreopithecus*) contrast with the longer CC and the rectangular-
378 shaped anterior canal found in *Hispanopithecus* (Fig. 1d). In these regards,
379 *Hispanopithecus* more closely resembles the members of the African ape and
380 human clade (Fig. 1a-c).

381 In summary, each extant hominid genus is derived in a particular direction from
382 the ancestral morphology, with *Pan* remaining close to the hominid and hominine
383 LCAs; *Nacholapithecus* appears as the least derived among both extant and fossil
384 hominid taxa, together with *Oreopithecus*. The latter taxon also shows similarities
385 with *Pongo* in the anterosuperiorly projecting anterior canal (Fig. 1e,j), despite being
386 much slenderer in *Oreopithecus*. Overall, the dryopiths appear less derived than
387 most extant genera relative to either the crown hominid or the crown hominine LCA,
388 irrespective of their preferred phylogenetic placement. *Rudapithecus* appears more
389 primitive than *Hispanopithecus*, being closer than the latter to both *Nacholapithecus*
390 and *Oreopithecus*, and closely approaching both the reconstructed crown hominid
391 LCA and *Pan* (Figs. 1, 5, 6). In contrast, *Hispanopithecus* is in some respects more
392 derived than *Rudapithecus*, particularly toward orangutans, australopiths, and
393 humans in the large vestibular recesses and in the stout SC volumetric proportions,
394 and toward orangutans alone in the rounded posterior canal morphology (Fig. 5).
395 Despite *Hispanopithecus* sharing its CC apex morphology (intermediate between
396 African great apes and orangutans) and anterior canal shape (not anterosuperiorly
397 projecting, yet not as squared as in gorillas) with *Homo* and *Australopithecus*, this

398 condition could be possibly plesiomorphic for hominids as a whole, as it is also found
399 in the stem hominid *Nacholapithecus* (Fig 5). Overall, the two dryopiths share with
400 African great apes and humans some features (moderately stout SCs, not
401 anterosuperiorly projecting anterior canal, fairly long CC), but according to our
402 analyses these features appear primitive (being likely present in the hominid LCA
403 and, to a lesser extent, *Nacholapithecus*), with hominines (particularly gorillas) and
404 especially orangutans having subsequently derived in opposite directions.

405

406 **Discussion**

407 Our results show that the vestibular morphology of both *Hispanopithecus* and
408 *Rudapithecus* more closely resembles that of extant great apes and humans than
409 that of hylobatids, in agreement with the current consensus that they belong to the
410 great-ape-and-human clade (2-3, 6, 26). These similarities particularly concern the
411 volumetric proportions of the SCs as well as the size of the latter relative to the
412 vestibular recesses. Volumetric proportions, as reflected by the ratio between the
413 volume and the length of the SCs, appear particularly relevant given that an
414 allometric grade shift has been previously identified to characterize all extant
415 hominids, so that they display relatively more voluminous SCs than other
416 anthropoids (including hylobatids) at comparable lengths (5). The derived condition
417 of hominids has been linked with locomotion (5), but is noteworthy that chimpanzees,
418 bonobos, and gorillas are slightly more variable in SC volumetric proportions than
419 orangutans and humans. Given the relationship between SC shape variation and
420 locomotion noted by some authors (53-54), our results might reflect stronger
421 locomotor-related selection pressures in orangutans and humans.

422 The classification results based on the bgPCA as well as the cluster analyses
423 indicate that the two investigated dryopiths are distinguishable from one another,
424 with the three specimens (two individuals) of *Rudapithecus* being more similar to one
425 another than to the single specimen of *Hispanopithecus*. This result, together with
426 other cranial differences (e.g., morphology of the frontal squama, premaxilla, and
427 zygomatic), supports the distinction of these taxa at the genus rank (2-3, 7, 21, 25,
428 35). *Rudapithecus* generally displays a somewhat more primitive morphology, closer
429 to the one inferred for the crown hominid LCA. It shows some similarities with the
430 fossil hominoids *Oreopithecus* and *Nacholapithecus*. The latter taxon appears more
431 primitive than other hominids, in agreement with a previous study based on the
432 entire inner ear morphology (49). However, both the hominid-like volumetric
433 proportions of *Nacholapithecus* and the lack of a subarcuate fossa (55) support its
434 stem hominid status, closely resembling the morphotype reconstructed for the crown
435 hominid LCA. The morphology of *Rudapithecus* also resembles that of crown
436 hominids such as *Pan* (volumetric proportions and the relative size of the SCs) and,
437 to a lesser extent, orangutans (the somewhat anterosuperiorly projecting anterior
438 canal and the short CC). As previously noted (5), chimpanzees and bonobos appear
439 least derived than other extant hominids. This is shown by the possession of
440 similarly-sized SCs (shared with the reconstructed crown hominid and crown
441 hominine LCAs, while the dryopith LCA displays a slightly smaller lateral canal) and,
442 especially, by the fairly slender volumetric proportions (intermediate between the
443 hominine and hominid LCAs, yet closer to the latter). This is also supported by the
444 similarities between *Pan* species and Miocene apes, especially *Nacholapithecus*.
445 Nonetheless, chimpanzees and bonobos appear derived in some features (the small
446 and rounded posterior canal as well as the obtuse angle of the CC apex), just like

447 gorillas and humans are derived in other directions (largest lateral canal relative to
448 the other SCs and markedly enlarged vertical canals, respectively). Among
449 hominids, orangutans and humans show the most extreme condition in the
450 volumetric proportions of the SCs. Orangutans further diverge from the hominid LCA
451 by the anterosuperiorly projecting anterior canal (even more so than in hylobatids).
452 *Hispanopithecus* appears more derived than the other Miocene taxa, especially by
453 the stouter SCs, while it does not fit well within the variation of any extant genus.
454 More clearly than *Rudapithecus*, *Hispanopithecus* displays a mosaic of features that
455 is unknown among extant hominids, including similarities with chimpanzees and
456 bonobos (in the long CC), humans (the obtuse angle of the CC apex and the right
457 angle between the planes of the posterior and lateral canals), and orangutans (the
458 stout CC and the voluminous vestibular recesses, the latter also shared with
459 humans) coupled with some unique features (the swollen area between the ampulla
460 and the tip of the lateral canal, and the markedly inflated ampullae).

461 Interpreting the similarities of the investigated dryopiths in evolutionary terms is
462 not straightforward. The results of the phylomorphospace approach and the
463 reconstructed ancestral vestibular morphologies suggest that modern hominid-like
464 volumetric proportions of the SCs would have been present in the LCA of crown
465 hominids, while that of crown hominoids as a whole would have displayed somewhat
466 intermediate proportions between hylobatids and hominids (yet closer to the latter).
467 Differences in volumetric proportions of the SCs have been related to locomotor
468 adaptations, because they directly affect the sensitivity and steadiness of the SCs in
469 response to angular accelerations (5, 56). Hence, the moderately stout SCs of the
470 LCA of crown hominids indicate that it showed a slow type of locomotion, which was
471 present, to a large extent, also in the LCA of crown hominoids, as previously inferred

472 based on the size of the SC radius alone (41). Both *Rudapithecus* and
473 *Hispanopithecus* show a wide gap between the lateral and posterior canals (the
474 planes defined by them are well separated and do not intersect), caused by the
475 anterolateral location of the lateral canal. This trait has been linked to orthograde
476 behaviors (42), in agreement with the fossil evidence available for these taxa (6, 11,
477 23, 25, 35, 57-61). However, from a phylogenetic viewpoint, the presence of the
478 aforementioned feature in the investigated dryopiths is less informative than their
479 hominid-like volumetric proportions, since the former have been identified as a
480 synapomorphy of crown hominoids as a whole (5).

481 We conclude that, with differences that are consistent with their distinction at the
482 genus rank, both *Hispanopithecus* and *Rudapithecus* display a unique hominid-like
483 vestibular morphology that differs from that of any extant hominid genera but that
484 appears quite close to that ancestral for crown hominids and crown hominines—
485 mainly diverging from that of hylobatids by the stouter volumetric proportions of the
486 SCs that are uniquely characteristic of great apes and humans among anthropoids.
487 Orangutans appear most derived from such an ancestral vestibular morphology,
488 whereas the investigated dryopiths lack most orangutan-like derived features—
489 except for the slightly anterosuperiorly projecting anterior canal in *Rudapithecus*
490 (also found in *Hylobates*) and some torsion in the shape of the lateral canal (a
491 character that appears to be quite variable within hominoids). The lack of orangutan
492 derived features in dryopithecines does not completely rule out a stem pongine
493 status, as previously supported by some authors (10, 29-30), as it represents a more
494 primitive morphology that probably precedes the subsequent evolution of the
495 orangutan-like features in the pongine lineage. However, our results are more
496 consistent with a stem hominid (6, 28) or a stem hominine (2-3, 14, 16, 25) status for

497 the investigated dryopiths. Our results suggest that African apes and hominin genera
498 evolved in different directions from an ancestral morphology that more closely
499 resembles that of *Pan* among extant hominines, and which is largely plesiomorphic
500 for hominids, as further supported by similarities with the stem hominid
501 *Nacholapithecus* (except for the slenderer volumetric proportions of the latter).
502 Therefore, similarities between the SC morphology of the studied dryopiths and that
503 of African apes do not necessarily imply a hominine status, but overall support the
504 previous claim (5), based on extant taxa alone, that extant hominines evolved from
505 an ancestral condition quite similar to that of the crown hominid LCA, and that the
506 latter was characterized by derived volumetric proportions of the SCs. Pending the
507 analysis of other Miocene apes, *Pan* among the extant taxa, and *Rudapithecus*
508 among extinct apes, constitute the best available proxies for such ancestral
509 morphologies, being already somewhat more derived from the crown hominoid
510 condition that is best approximated by *Nacholapithecus*. In the future, the inclusion in
511 the analyses of additional extinct hominoids will hopefully clarify further the
512 evolutionary history of this hominoids during the Miocene.

513

514 **Materials and Methods**

515 **Sample Composition and Acquisition.** We inspected three petrosals from two
516 individuals of *R. hungaricus* from Rudabánya, Hungary (RUD 77, left [RUD 77L] and
517 right [RUD 77R]; and RUD 200, right) (12-13) and the single available petrosal of *H.*
518 *laietanus* from Can Llobateres 2, Spain (IPS18000, right) (10, 29-30). The
519 specimens of *Rudapithecus* are housed at the Geological Museum of the Mining and
520 Geological Survey of Hungary (Hungary) and were scanned with a Skyscan 1172
521 (obtaining a resolution of 0.0136 mm) at the Max Plank Institute for Evolutionary

522 Anthropology (Leipzig, Germany), with the following parameters: 100 kV voltage and
523 100 mA. In turn, IPS18000 is housed at the Institut Català de Paleontologia Miquel
524 Crusafont in Sabadell (Spain) and was scanned with a GE Phoenix V|Tome|X s 240
525 (obtaining a resolution of 0.0295 mm) at the Centro Nacional de Investigación sobre
526 la Evolución Humana (Burgos, Spain), with the following parameters: 125 kV voltage
527 and 120 mA. The 3D virtual models of IPS18000, RUD 200 and RUD 77R were
528 mirrored to enable the comparison with extant species. The segmented surfaces of
529 the SCs of these fossils are available from MorphoSource
530 (<https://www.morphosource.org>; see Supplementary Table 3).

531 The comparative sample for the volumetric proportion evaluation has been taken
532 from a previous analysis that evaluated the phylogenetic signal embedded in the
533 vestibule morphology (5), and integrated with recently published material of extant
534 hominoids (4) and humans (62), together with the stem hominid *Nacholapithecus*
535 *kerioi* (49). Overall, it consists of μ CT scans of 169 dried crania and petrosals
536 belonging to 27 extant anthropoid species, including all hominid genera and a
537 selection of hylobatids, cercopithecoids, and platyrrhines, together with fossil taxa
538 (Supplementary Table 3). The 3D meshes of the inner ear bony labyrinth of StW 573
539 and StW 578 were downloaded from the Sterkfontein project of the digital repository
540 MorphoSource.org. The juvenile status of a few specimens should not affect their
541 vestibular morphology since the bony labyrinth ossifies in early prenatal stages and
542 does not change subsequently (63). The analysis of the patterns of shape variation
543 was focused on hominoids alone and was based on a subsample of 77 individuals
544 representing all extant hominoid genera (Supplementary Table 4).

545 The μ CT scans (voxel size for the extant and fossil specimens added in the
546 present analysis to those originally published in ref. 5 can be found in in

547 Supplementary Table 5) were segmented using Avizo 9.0.1 (FEI Visualization
548 Sciences Group) to digitally extract the left bony labyrinth, when available, or that
549 from the right side (mirrored before the surface alignment). The vestibular apparatus
550 was separated from the cochlea by cutting the generated 3D surfaces right under the
551 saccule and the oval window and filling the resulting holes with Geomagic Studio
552 2014 (3D Systems) using a flat surface (5).

553 The anatomical axes used for describing semicircular canal morphology
554 corresponds to those employed in the vast majority of inner ear analysis focusing on
555 primates (36-37,42,49), which conventionally follow the same orientation as in
556 humans (i.e., superior/inferior and anterior/posterior).

557 **Shape Analysis.** Shape was analyzed using a deformation-based 3DGM
558 technique that does not rely on a priori defined landmarks and examines the
559 geometrical correspondences between continuous surfaces (5, 48, 64-66). This
560 method quantifies the deformation from the analyzed surfaces from a constructed
561 sample-average surface (template) (64, 66), mathematically models them as a
562 diffeomorphism, and computes a set of vectors (momenta) that describe the direction
563 and magnitude of deformation from the average template. The unscaled 3D models
564 were aligned with Avizo 9.0.1 using the 'Align Surface' module before running the
565 analyses. The diffeomorphisms and the momenta were computed in the Barcelona
566 Supercomputing Center (BSC) (Barcelona, Spain) with Deformetrica 4 software. The
567 3D models of the fossils were projected a posteriori in the tangent space generated
568 by means of between-group principal components analysis (bgPCA) ran on the set
569 of momenta for the hominoid-only sample using genera as grouping factor. The
570 bgPCA was computed in R Studio v.1.1.453 for R v.3.5.0 using the *ade4* package
571 (67), while the cross-validated bgPCA was derived using the 'groupPCA' function of

572 the *Morpho* v2.6 (68) library. Group mean differences were tested by computing a
573 permutational ANOVA (1000 permutations) based on the Euclidean distance
574 between the means using the 'adonis' function of the *Vegan* package (69). The
575 amount of variance (R^2) explained by group differences in the raw shape data, and in
576 the scores of both standard and cross-validated bgPCA results, was estimated with
577 the same function as for the permutation test. To further assess similarities between
578 the analyzed fossil taxa and extant hominoid genera in terms of vestibular
579 morphology, we computed Mahalanobis squared distances (D^2) between the bgPC
580 scores of fossils and group centroids used in the bgPCA. The distances were also
581 used to compute the posterior probabilities of group membership for the fossil
582 specimens by means of the 'typprobClass' function of the *Morpho* v2.6 (68) package,
583 on the basis of the multivariate normal distribution of extant groups defined a priori in
584 the bgPCA analyses. The similarities between extant and fossil hominoids were
585 further investigated by means of a cluster analysis (UPGMA) on the aforementioned
586 D^2 and on the Euclidean distances between pairs of species mean configurations for
587 the raw data using the 'average' method of the 'hclust' function of the 'stats' package
588 in R

589 Additionally, the correlation between the log-transformed cube root of SC volume
590 ($\ln \text{VolSC}$, in mm) and log-transformed SC length ($\ln L$, in mm) was assessed means
591 of ordinary least-squares (OLS) linear regression, as the relationship between these
592 variables has previously been shown to display an allometric grade shift between
593 hominids and other anthropoids (5). Two separate regressions were computed for
594 the non-hominid anthropoids and for great apes and humans using SPSS Statistics
595 v. 17.0 for Windows (see Fig. 7b in ref. 5). The regression for the non-hominid
596 sample was used as a baseline for computing the allometric residuals

597 (Supplementary Table 1; see Table 5 in ref. 5) for the extant and extinct species.
598 Comparisons between the latter and extant groups are depicted by means of box-
599 and-whisker plots.

600

601 **Phylomorphospace and phylogenetic signal.** Major patterns of vestibular shape
602 variation were quantified using a phylomorphospace approach (70), obtained by
603 projecting a phylogeny on to the tangent space derived from the bgPCA of a 3DGM
604 shape analysis. In this method, the tips of the phylogeny correspond to the genus
605 bgPC centroid, while the internal nodes (i.e., the ancestral states) of the tree are
606 estimated using a maximum likelihood method for continuous characters, assuming
607 that the reconstructed nodes approximate the true morphology of the ancestors.
608 Thus, when a time-calibrated phylogeny is used, its two-dimensional representation
609 enables the intuitive interpretation of the magnitude and direction of evolution, based
610 on branch length and orientation. The molecular-based phylogenetic tree for extant
611 hominoids used in this analysis was downloaded from the 10kTrees Website (ver. 3;
612 <http://10ktrees.fas.harvard.edu/>), while *Hispanopithecus* and *Rudapithecus* were
613 added based on the assumption that they are closely related and constitute a clade,
614 with the tips corresponding to 9.6 Ma and 10.1 Ma, respectively (20), and diverging
615 at 11.1 Ma, but considering three different phylogenetic placements for these taxa as
616 discussed in the literature during the last two decades (see above): stem hominids,
617 stem hominines, and stem pongines (Supplementary Fig. 2). Analyses were
618 repeated based on the resulting three different cladograms and their results
619 compared to evaluate the effect of phylogenetic uncertainties surrounding these
620 taxa. *Oreopithecus* is here considered as a stem hominoid as indicated by most
621 recent cladistic analyses (4). *Nacholapithecus* has been included in a stem hominid

622 position, 2 Myr older than the divergence between pongines and hominines (crown
623 hominids), thus always preceding the divergence of dryopiths in all the phylogenetic
624 hypotheses, and its tip corresponds to 14.77 Ma (54, 71). The divergence between
625 crown hominoids and *Oreopithecus* has been placed 1 Myr older than the
626 divergence between hylobatids and hominids and its tip corresponds to its last
627 occurrence in the fossil record (7.0-6.5 Ma; ref. 72). For the South African
628 *Australopithecus* sp., we used the published first appearance datum for
629 *Australopithecus africanus* (4.02 Ma) that includes the Jacovec specimens into the
630 species (73).

631 The position in the morphospace of the internal nodes of the phylogeny (ancestral
632 morphologies) was estimated via a maximum likelihood method for continuous
633 characters (74) using the 'fastAnc' function of *phytools* v. 0.6-60 R package (75).
634 Subsequently, the bgPC scores of the ancestral states were rotated and translated
635 from the shape data back into the configuration space for interpolation and 3D
636 visualization using Deformetrica 3 software.

637 The phylogenetic signal embedded in vestibular shape, as captured by all the
638 bgPCs, was quantified by means of the multivariate phylogenetic index K_{mult} (76)
639 using *geomorph* v3.1.1 (77) R package. The K_{mult} statistic, like its univariate
640 counterpart (77), assesses the amount of phylogenetic signal relative to that
641 expected for character undergoing Brownian motion and reflects the accuracy with
642 which the phylogenetic tree describes the variance-covariance pattern found in the
643 shape data. It is also informative about the accumulation of the variance in the
644 phylogeny. Thus, $K_{\text{mult}} \approx 1$ is obtained when the inspected mode of evolution can
645 adequately be described using a stochastic Brownian motion model. For $K_{\text{mult}} < 1$,
646 the majority of the variance is found within clades, thus implying that neighbor taxa

647 resemble one another less than expected and that the mode of evolution is not
648 aleatory, possibly as the results of homoplastic adaptations (i.e., related to function
649 rather than phylogeny). Values of $K_{\text{mult}} > 1$ indicate that variance is mostly found
650 among different clades, being obtained when close taxa are less diverse than
651 expected under Brownian motion (suggesting that phenomena of stabilizing selection
652 might have occurred).

653

654 **Acknowledgements**

655 This research has been funded by the Agencia Estatal de Investigación (CGL2016-
656 76431-P and CGL2017-82654-P, AEI/FEDER EU; and BES-2015-071318 to A.U.),
657 the Generalitat de Catalunya (CERC A Programme), the consolidated research
658 groups 2017 SGR 86 and 2017 SGR 116 GRC, and the French Centre National de
659 la Recherche Scientifique. Part of the analyses were performed using Barcelona
660 Supercomputing Center resources (BCV-2020-1-0008). We thank Jose Braga for
661 allowing us to use the CT scans of the human specimens; the Max Plank Institute for
662 providing access to the microCT scans of RUD 77 and RUD 200; the ESRF heritage
663 database for palaeontology, evolutionary biology and archaeology, for providing
664 access to a part of the hominoid scans used in the present analysis; and Lynn
665 Copes, Lynn Lucas, and the Museum of Comparative Zoology (Cambridge, MA) for
666 providing access to a part of the scans used in the study, originally appearing in refs.
667 79 and 80, and funded by NSF DDIG #0925793, and a Wenner-Gren Foundation
668 Dissertation Grant #8102 (both to Lynn Copes). These scans were downloaded from
669 MorphoSource.org, a web-accessible archive for 3D digital data housed by Duke
670 University. A.B. was funded by the University of the Witwatersrand.

671

672 **References**

- 673 1. N. J. Stevens, et al., Palaeontological evidence for an Oligocene divergence
674 between Old World monkeys and apes. *Nature* **497**, 611–614 (2013).
- 675 2. D. R. Begun, “The Miocene hominoid radiation“ in A companion to
676 Paleoanthropology D. R. Begun, Ed. (Blackwell Publishing, 2013), pp. 398–
677 416.
- 678 3. D. R. Begun, “Fossil record of Miocene hominoids” in Handbook of
679 Paleoanthropology, 2nd edn, W. Henke, I. Tattersall, Eds. (Springer, 2015),
680 pp. 1261–1332.
- 681 4. I. Nengo, et al., New infant cranium from the African Miocene sheds light on
682 ape evolution. *Nature* **548**, 169–174 (2017).
- 683 5. A. Urciuoli, C. Zanolli, J. Dumoncel, S. Moyà-Solà, D. M. Alba, The evolution
684 of the vestibular apparatus in apes and humans. *eLife* **9** (2020)
- 685 6. D. M. Alba, Fossil apes from the Vallès-Penedès Basin. *Evol. Anthropol.* **21**,
686 254–269 (2012).
- 687 7. Begun, D. R. Miocene hominids and the origins of the African apes and
688 humans. *Ann. Rev. Anthropol.* **39**, 67–84 (2010).
- 689 8. J. Kelley, “The hominoid radiation in Asia” in The Primate Fossil Record, W.
690 C. Hartwig, Ed. (Cambridge University Press, 2002), pp. 369–384.
- 691 9. P. Andrews, T. Harrison, E. Delson, R. L. Bernor, L. Martin, “Distribution and
692 biochronology of European and Southwest Asian Miocene catarrhines” in The
693 Evolution of Western Eurasian Neogene Mammal Faunas, R. L. Bernor, V.
694 Fahlbusch & H.-W. Mittmann, Eds. (Columbia University Press, 1996), pp.
695 168–207.

- 696 10. S. Moyà-Solà, M. Köhler, Recent discoveries of *Dryopithecus* shed new light
697 on evolution of great apes. *Nature* **365**, 543 (1993).
- 698 11. S. Moyà-Solà, M. Köhler, A *Dryopithecus* skeleton and the origins of great-
699 ape locomotion. *Nature* **379**, 156–159 (1996).
- 700 12. L. Kordos, Begun, R. D., A new reconstruction of RUD 77, a partial cranium of
701 *Dryopithecus brancoi* from Rudabánya, Hungary. *Am. J. Phys. Anthropol.*
702 **103**, 277–294 (1997).
- 703 13. L. Kordos, D. R. Begun, A new cranium of *Dryopithecus* from Rudabánya,
704 Hungary. *J. Hum. Evol.* **41**, 689–700 (2001).
- 705 14. D. R. Begun, C. V. Ward, M. D. Rose, “Events in hominoid evolution” in
706 Function, Phylogeny and Fossils: Miocene Hominoid Evolution and
707 Adaptation, D. R. Begun, C. V. Ward, M. D. Rose (Plenum Press, 1997), pp.
708 389–415.
- 709 15. D. R. Begun, “African and Eurasian Miocene hominoids and the origins of the
710 Hominidae” in Hominoid Evolution and Environmental Change in the Neogene
711 of Europe, Vol 2. Phylogeny of the Neogene Hominoid Primates of Eurasia, L.
712 D. Bonis, G. Koufos, P. Andrews, Eds. (Cambridge University Press, 2001),
713 pp. 231–253.
- 714 16. D. R. Begun, “The pliopithecoidea” in: The Primate Fossil Record, W. Hartwig,
715 Ed. (Cambridge University Press., 2002), pp. 339–368.
- 716 17. S. Moyà-Solà, M. Köhler, D. M. Alba, I. Casanovas-Vilar, J. Galindo,
717 *Pierolapithecus catalaunicus*, a new Middle Miocene great ape from Spain.
718 *Science* **306**, 1339–1344 (2004).
- 719 18. S. Moyà-Solà, et al., First partial face and upper dentition of the Middle
720 Miocene hominoid *Dryopithecus fontani* from Abocador de Can Mata (Vallès-

- 721 Penedès Basin, Catalonia, NE Spain): taxonomic and phylogenetic
722 implications. *Am. J. Phys. Anthropol.* **139**, 126–145 (2009).
- 723 19. S. Moyà-Solà, et al., A unique Middle Miocene European hominoid and the
724 origins of the great ape and human clade. *Proc. Natl. Acad. Sci. U.S.A.* **106**,
725 9601–9606 (2009).
- 726 20. I. Casanovas-Vilar, et al., Updated chronology for the Miocene hominoid
727 radiation in Western Eurasia. *Proc. Natl. Acad. Sci. U.S.A.* **108**, 5554–5559
728 (2011).
- 729 21. D. R. Begun, Dryopithecins, Darwin, de Bonis, and the European origin of the
730 African apes and human clade. *Geodiversitas* **31**, 789–816 (2009).
- 731 22. D. M. Alba, et al., New dental remains of *Hispanopithecus laietanus*
732 (Primates: Hominidae) from Can Llobateres 1 and the taxonomy of Late
733 Miocene hominoids from the Vallès-Penedès Basin (NE Iberian Peninsula). *J.*
734 *Hum. Evol.* **63**, 231–246 (2012).
- 735 23. D. M. Alba, S. Almécija, I. Casanovas-Vilar, J. M. Méndez, S. Moyà-Solà, A
736 partial skeleton of the fossil great ape *Hispanopithecus laietanus* from Can
737 Feu and the mosaic evolution of crown-hominoid positional behaviors. *PLoS*
738 *ONE* **6**, e39617 (2012).
- 739 24. D. R. Begun, *Sivapithecus* is east and *Dryopithecus* is west, and never the
740 twain shall meet. *Anthropol. Sci.* **113**, 53–64 (2005).
- 741 25. D. R. Begun, M. C. Nargolwalla, L. Kordos, European Miocene hominids and
742 the origin of the African ape and human clade. *Evol. Anthropol.* **21**, 10–23
743 (2012).
- 744 26. P. Andrews, Last common ancestor of apes and humans: morphology and
745 environment. *Folia Primatol.* **91**, 1–27 (2020).

- 746 27. M. Böhme, et al. A new Miocene ape and locomotion in the ancestor of great
747 apes and humans. *Nature* **575**, 489–493 (2019).
- 748 28. D. M. Alba, et al., Miocene small-bodied ape from Eurasia sheds light on
749 hominoid evolution. *Science* **350**, aab2625 (2015).
- 750 29. M. Köhler, S. Moyà-Solà, D. M. Alba, “Eurasian hominoid evolution in the light
751 of recent *Dryopithecus* findings” in: Hominoid Evolution and Environmental
752 Change in the Neogene of Europe, Vol 2. Phylogeny of the Neogene
753 Hominoid Primates of Eurasia, L. D. Bonis, G. Koufos, P. Andrews, Eds.
754 (Cambridge University Press, 2001), pp. 192–212.
- 755 30. S. Moyà-Solà, M. Köhler, New partial cranium of *Dryopithecus* Lartet, 1863
756 (Hominoidea, Primates) from the upper Miocene of Can Llobateres,
757 Barcelona, Spain. *J. Hum. Evol.* 29, 101–139 (1995).
- 758 31. D. R. Begun, L. Kordos, “Phyletic affinities and functional convergence in
759 *Dryopithecus* and other Miocene and living hominids.” in Function, Phylogeny,
760 and Fossils: Miocene Hominoid Evolution and Adaptions, D.R., Begun, C.V.,
761 Ward, M.D., Rose Eds. (Plenum Press, 1997), pp. 291–316.
- 762 32. D. R. Begun, How to identify (as opposed to define) a homoplasy: Examples
763 from fossil and living great apes. *J. Hum. Evol.* **52**, 559–572 (2007).
- 764 33. S. G. Larson, Parallel evolution in the hominoid trunk and forelimb. *Evol.*
765 *Anthropol.* **6**, 87–99 (1998).
- 766 34. T. C. Rae, Mosaic evolution in the origin of the Hominoidea. *Folia Primatol.*
767 **70**, 125–135 (1999).
- 768 35. C. V. Ward, “Postcranial and locomotor adaptations of hominoids” in
769 Handbook of Paleoanthropology, 2nd edn W. Henke, I. Tattersall, Eds.
770 (Springer, 2015), pp. 1363–1386.

- 771 36. F. Spoor, B. Wood, F. Zonneveld, Implications of early hominid labyrinthine
772 morphology for evolution of human bipedal locomotion. *Nature* **369**, 645–648
773 (1994).
- 774 37. F. Spoor, F. Zonneveld, Comparative review of the human bony labyrinth.
775 *Yearb. Phys. Anthropol.* **41**, 211–251 (1998).
- 776 38. Spoor, F. et al., The primate semicircular canal system and locomotion. *Proc.*
777 *Natl. Acad. Sci U.S.A.* **104**, 10808–10812 (2007).
- 778 39. David, R., et al., Motion from the past. A new method to infer vestibular
779 apparatus capacities of extinct species. *C. R. Palevol* **9**, 397–410 (2010).
- 780 40. David, R., A. Stoessel, A. Berthoz, F. Spoor, D. Bennequin, Assessing
781 morphology and function of the semicircular duct system: introducing new in-
782 situ visualization and software toolbox. *Sci. Rep.* **6**, 32772 (2016).
- 783 41. T. M. Ryan, et al., Evolution of locomotion in Anthroidea: the semicircular
784 canal evidence. *Proc. R. Soc. B* **279**, 3467–3475 (2012).
- 785 42. A. Le Maître, P. Schuetz, P. Vignaud, M. Brunet, New data about semicircular
786 canal morphology and locomotion in modern hominoids. *J. Anat.* **231**, 95–109
787 (2017).
- 788 43. L. Rook, et al., The bony labyrinth of *Oreopithecus bambolii*. *J. Hum. Evol.* **46**,
789 347–354 (2004).
- 790 44. M. S. Ponce de León, et al., Human bony labyrinth is an indicator of
791 population history and dispersal from Africa. *Proc. Natl. Acad. Sci. U.S.A.* **115**,
792 4128–4133 (2018).
- 793 45. A. Beaudet, The inner ear of the *Paranthropus* specimen DNH 22 from
794 Drimolen, South Africa. *Am. J. Phys. Anthropol.* **170**, 439–446 (2019).

- 795 46. A. Beaudet, et al., The bony labyrinth of StW 573 (“Little Foot”): Implications
796 for early hominin evolution and paleobiology. *J. Hum. Evol.* **127**, 67–80
797 (2019).
- 798 47. J. del Rio, et al., Allometry, function and shape diversification in the inner ear
799 of platyrrhine primates. *J. Mammal. Evol.* (2020) DOI:
800 <https://doi.org/10.1007/s10914-019-09490-9>
- 801 48. A. Urciuoli, C. Zanolli, S. Almécija, S. Moyà-Solà, D. M. Alba, Analysis of the
802 primate vestibular apparatus: a comparison of landmark-based and
803 deformation-based 3D geometric morphometric approaches. *Proc. Eur. Soc.*
804 *Stud. Hum. Evol.* **7**, 193 (2018).
- 805 49. N. Morimoto, et al., Variation of bony labyrinthine morphology in
806 Mio–Plio–Pleistocene and modern anthropoids. *Am. J. Phys. Anthropol.* **173**,
807 276–293 (2020)
- 808 50. T. C. Rae, P. M. Johnson, W. Yano, E. Hirasaki, Semicircular canal size and
809 locomotion in colobine monkeys: a cautionary tale. *Folia Primatol.* **87**, 213–
810 223 (2016).
- 811 51. D. M. Malinzak, R. F. Kay, T. E. Hullar, Locomotor head movements and
812 semicircular canal morphology in primates. *Proc. Natl. Acad. Sci. U.S.A.* **109**,
813 17914–17919 (2012).
- 814 52. A. Cardini, P. D. Polly, Cross-validated between-group PCA scatterplots: A
815 solution to spurious group separation? *Evol. Biol.* **47**, 85–95 (2020).
- 816 53. A. Perier, R. Lebrun, L. Marivaux, Different level of intraspecific variation of
817 the bony labyrinth morphology in slow- versus fast-moving Primates. *J.*
818 *Mammal. Evol.* **23**, 353–368 (2016).

- 819 54. L. A. Gonzales, M. D. Malinzak, R. F. Kay, Intraspecific variation in
820 semicircular canal morphology—A missing element in adaptive scenarios?
821 *Am. J. Phys. Anthropol.* **168**, 10–24 (2019).
- 822 55. Y. Kanimatsu, M. Nakatsukasa, D. Shimizu, Y. Nakano, H. Ishida, Loss of the
823 subarcuate fossa and the phylogeny of *Nacholapithecus*. *J. Hum. Evol.* **131**,
824 22–27 (2019).
- 825 56. R. D. Rabbitt, E. R. Damiano, J. W. Grant, “Biomechanics of the Semicircular
826 Canals and Otolith Organs” in *The Vestibular System* S. M. Highstein, R. R.
827 Fay, A. N. Popper, Eds. (Springer, 2004) pp. 153–201.
- 828 57. D. R. Begun, Phyletic diversity and locomotion in primitive European
829 hominids. *Am. J. Phys. Anthropol.* **87**, 311–340 (1992).
- 830 58. D. R. Begun, New catarrhine phalanges from Rudabánya (Northeastern
831 Hungary) and the problem of parallelism and convergence in hominoid
832 postcranial morphology. *J. Hum. Evol.* **24**, 373–402 (1993).
- 833 59. S. Almécija, D. M. Alba, S. Moyà-Solà, M. Köhler, Orang-like manual
834 adaptations in the fossil hominoid *Hispanopithecus laietanus*: first steps
835 towards great ape suspensory behaviours. *Proc. R. Soc. B* **274**, 2375–2384
836 (2007).
- 837 60. D. M. Alba, S. Almécija, S. Moyà-Solà, Locomotor inferences in
838 *Pierolapithecus* and *Hispanopithecus*: reply to Deane and Begun (2008). *J.*
839 *Hum. Evol.* **59**, 143–149 (2010).
- 840 61. M. Pina, D. M. Alba, S. Almécija, J. Fortuny, S. Moyà-Solà, Brief
841 communication: paleobiological inferences on the locomotor repertoire of
842 extinct hominoids based on femoral neck cortical thickness: the fossil great

- 843 ape *Hispanopithecus laietanus* as a test-case study. *Am. J. Phys. Anthropol.*
844 **149**, 142–148 (2012).
- 845 62. W. Wimmer, C. Vandersteen, N. Guevara, M. Caversaccio, H. Delingette, H.,
846 “Robust cochlear modiolar axis detection in CT” in *Medical Image Computing*
847 *and Computer Assisted Intervention – MICCAI 2019* D. Shen, et al. Eds.
848 (Springer, 2019), pp. 3–10.
- 849 63. N. Jeffery, F. Spoor, Prenatal growth and development of the modern human
850 labyrinth. *J. Anat.* **204**, 71–92 (2004).
- 851 64. S. Durrleman, et al., “Topology preserving atlas construction from shape data
852 without correspondence using sparse parameters” in *Proceedings of Medical*
853 *Image Computing and Computer Aided Intervention* N. Ayache, H. Delingette,
854 P. Golland, K. Mori (Springer, 2012), pp. 223–230.
- 855 65. J. Dumoncel, S. Durrleman, J. Braga, J. P. Jessel, G. Subsol, Landmark-free
856 3D method for comparison of fossil hominins and hominids based on
857 endocranium and EDJ shapes. *Am. J. Phys. Anthropol.* **153**, 114 (2014).
- 858 66. A. Beaudet, et al., Upper third molar internal structural organization and
859 semicircular canal morphology in Plio-Pleistocene South African
860 cercopithecoids. *J. Hum. Evol.* **95**, 104–120 (2016).
- 861 67. S. Dray, A. Dufour, The ade4 Package: Implementing the duality diagram for
862 ecologists. *J. Stat. Softw.* **22**, (2007).
- 863 68. S. Schlager, “Morpho and Rvcg - Shape Analysis in R.” in: *Statistical Shape*
864 *and Deformation Analysis*, G. Zheng, S. Li, G. Szekely Eds. (Academic
865 Press., 2017) pp. 217–256.
- 866 69. J. Oksanen, et al., *vegan: Community Ecology Package*. R package version
867 2.5-6. <https://CRAN.R-project.org/package=vegan>

- 868 70. B. Sidlauskas, Continuous and arrested morphological diversification in sister
869 clades of characiform fishes: A phylomorphospace approach. *Evolution* **62**,
870 3135–3156 (2008).
- 871 71. M. Nakatsukasa, Y. Kunimatsu, *Nacholapithecus* and its importance for
872 understanding hominoid evolution. *Evol. Anthropol.* **18**, 103–119 (2009).
- 873 72. L. Rook, L. Bondioli, M. Köhler, S. Moyà-Solà, R. Macchiarelli, *Oreopithecus*
874 was a bipedal ape after all: evidence from the iliac cancellous architecture.
875 *Proc. Natl. Acad. Sci U.S.A.* **96**, 8795–8799 (1999).
- 876 73. B. Wood, E. K. Boyle, Hominin taxic diversity: Fact or fantasy? *Am. J. Phys.*
877 *Anthropol.* **159**, 37–78 (2016).
- 878 74. D. Schluter, T. Price, A. Ø. Mooers, D. Ludwig, Likelihood of ancestor states
879 in adaptive radiation. *Evolution* **51**, 1699–1711 (1997).
- 880 75. L. J. Revell, phytools: An R package for phylogenetic comparative biology
881 (and other things). *Methods Ecol. Evol.* **3**, 217–223 (2012).
- 882 76. D. C. Adams, A generalized K statistic for estimating phylogenetic signal from
883 shape and other high-dimensional multivariate data. *Syst. Biol.* **63**, 685–697
884 (2014).
- 885 77. D. C. Adams, M. L. Collyer, A. Kaliontzopoulou, Geomorph: Software for
886 geometric morphometric analyses. R package version 3.1.0. [https://cran.r-](https://cran.r-project.org/package=geomorph)
887 [project.org/package=geomorph](https://cran.r-project.org/package=geomorph) (2019).
- 888 78. S. P. Blomberg, J. T. Garland, A. R. Ives, Testing for a phylogenetic signal in
889 comparative data: behavioural traits are more labile. *Evolution* **57**, 717–745
890 (2003).
- 891 79. L. E. Copes, W. H. Kimbel, Cranial vault thickness in primates: *Homo erectus*
892 does not have uniquely thick vault bones. *J. Hum. Evol.* **90**, 120–134 (2016).

893 80. L. E. Copes, L. M. Lucas, J. O. Thostenson, H. E. Hoekstra, A collection of
894 non-human primate computed tomography scans housed in MorphoSource, a
895 repository for 3D data. *Sci. Data* **3**, 1 (2016).

896 **FIGURE CAPTIONS**

897 **Fig. 1.** The vestibular apparatus morphology of *Rudapithecus hungaricus* (**a-c**),
898 *Hispanopithecus laietanus* (**d**), fossil hominoids (**e-f**), and individuals from extant
899 hominoid genera (**g-m**) as depicted by renderings of the 3D models. From left to
900 right, in posterolateral, superior, and posteromedial views: (**a**) *R. hungaricus* (RUD
901 77L); (**b**) *R. hungaricus* (RUD 77R); (**c**) *R. hungaricus* (RUD 200); (**d**) *H. laietanus*
902 (IPS18000); (**e**) *Oreopithecus bambolii* (BAC 208); (**f**) *Nacholapithecus kerioi* (BG
903 42744); (**g**) *Hoolock hoolock* (AMNH.M 83425); (**h**) *Symphalangus syndactylus*
904 (AMNH.M 106583); (**i**) *Hylobates lar* (MCZ 41424); (**j**) *Pongo* sp.(IPS10647); (**k**)
905 *Gorilla gorilla* (AMNH.M 167338); (**l**) *Pan troglodytes* (AMNH.M 51204); (**m**) *Homo*
906 *sapiens* (F 04). Scale bars = 5 mm

907

908 **Fig. 2.** (**a**) Allometric regressions of cube root of semicircular canal volume (In
909 VolSC, in mm) vs. semicircular canal length (In L, in mm) in anthropoids. Lines
910 represent ordinary least-squares (OLS) best-fit lines for extant hominids (red) and
911 other extant anthropoids (blue). Both hominids and other anthropoids show a
912 negatively allometric relationship between VolSC and L, but with a marked allometric
913 grade shift—such that hominids possess stouter canals than other anthropoid taxa at
914 comparable lengths (see Supplementary Table 1 for comparative sample
915 measurements). (**b**) Boxplots of allometric residuals computed using the best-fit line
916 of the non-hominid anthropoid regression as baseline. Horizontal line is the median,
917 boxes represent the interquartile range, whiskers represent maximum and minimum
918 excluding outliers (beyond 1.5 times the upper and lower quartiles), and black dots
919 are outliers. Samples for each boxplot are: Platyrrhini ($n=15$), Cercopithecoidea
920 ($n=80$), Hylobatidae ($n=23$), *Gorilla* ($n=8$), *Pongo* ($n=8$), *Pan* ($n=25$), and *Homo*

921 ($n=10$). Note that all the fossils overlap with extant hominoids. However, while
922 *Australopithecus* (StW 573 and StW 578) and *Hispanopithecus* (IPS18000)
923 approach the human and orangutan condition, *Rudapithecus* RUD 200 and
924 *Oreopithecus* (BAC 208) only overlap with African apes, while *Nacholapithecus* (BG
925 42744) and *Rudapithecus* RUD 77 only overlap with chimpanzees and bonobos, and
926 marginally also with the upper range of hylobatids and cercopithecoids.

927

928 **Fig. 3.** Results of the bgPCA based on vestibular shape (as reflected by deformation
929 data) in hominoids using genera as grouping factor (variance explained by each
930 bgPC is included within parentheses): (a) bgPC2 vs. bgPC1; (b) bgPC3 vs. bgPC1.
931 Extreme conformations for each bgPC are displayed: (c) bgPC1; (d) bgPC2; (e)
932 bgPC3. Convex hulls are drawn for each hominoid genus and colored as follows:
933 blue, *Pongo*; black, *Gorilla*; green, *Pan*; lilac, *Homo*; red, *Hylobates*; orange,
934 *Symphalangus*; cyan, *Hoolock*.

935

936 **Fig. 4.** Dendrograms resulting from UPGMA cluster analyses based on: (a) the
937 Mahalanobis squared distances (D^2) computed for the meaningful between-group
938 principal components (bgPC1–bgPC3, 86% of variance) depicted in Figure 2
939 (cophenetic correlation: 0.75); (b) the Euclidean distances computed for the raw
940 shape data (i.e., the deformation fields) obtained from the deformation-based 3D
941 geometric morphometrics analysis (cophenetic correlation: 0.77).

942

943 **Fig. 5.** Phylomorphospaces of the vestibular apparatus in hominoids, obtained by
944 projecting the phylogenetic tree that considers dryopithecines a clade of stem
945 hominines (Supplementary Fig. 1b) on bivariate plots between bgPCs. The tips

946 correspond to genus bgPCA score centroids: **(a)** bgPC2 vs. bgPC1; **(b)** bgPC3 vs.
947 bgPC1. Key ancestral morphologies reconstructed using maximum likelihood for the
948 last common ancestors (LCAs) of various clades are depicted by means of
949 arrowheads. See Supplementary Fig. 2 for the results based on alternative
950 phylogenetic hypotheses (Supplementary Fig. 1a,c).

951

952 **Fig. 6.** Reconstructed vestibular shape for the last common ancestor (LCA) of the
953 main clades of interest as inferred using maximum likelihood methods for
954 deformation-based 3DGM analyses applied to the hominoid sample under the stem-
955 hominine phylogenetic hypothesis for dryopiths (Supplementary Fig. 1b), in
956 posterolateral (left), superior (middle), and posteromedial (right) views. The
957 reconstructed LCAs depicted are the following: **(a)** crown hominoids; **(b)** crown
958 hominids; **(c)** crown hominines; **(d)** dryopithecines (*Hispanopithecus* +
959 *Rudapithecus*). The results for the other phylogenetic hypotheses (not shown) are
960 virtually identical

a) *Rudapithecus* RUD 77L



b) *Rudapithecus* RUD 77R



c) *Rudapithecus* RUD 200



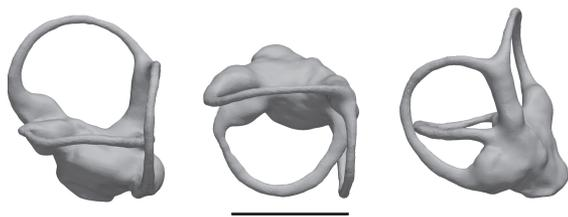
d) *Hispanopithecus* IPS18000



e) *Oreopithecus*



f) *Nacholapithecus*



g) *Hoolock*



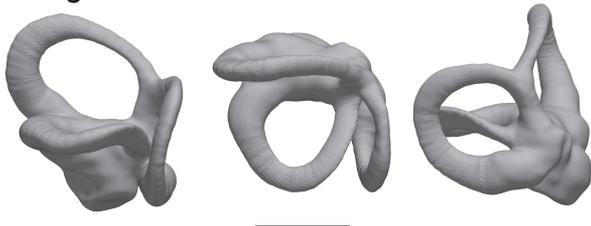
h) *Symphalangus*



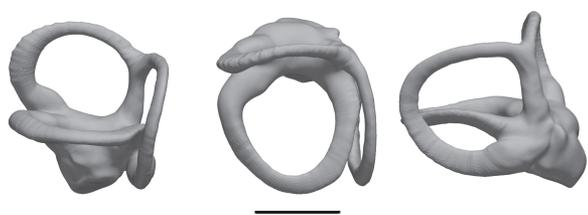
i) *Hylobates*



j) *Pongo*



k) *Gorilla*

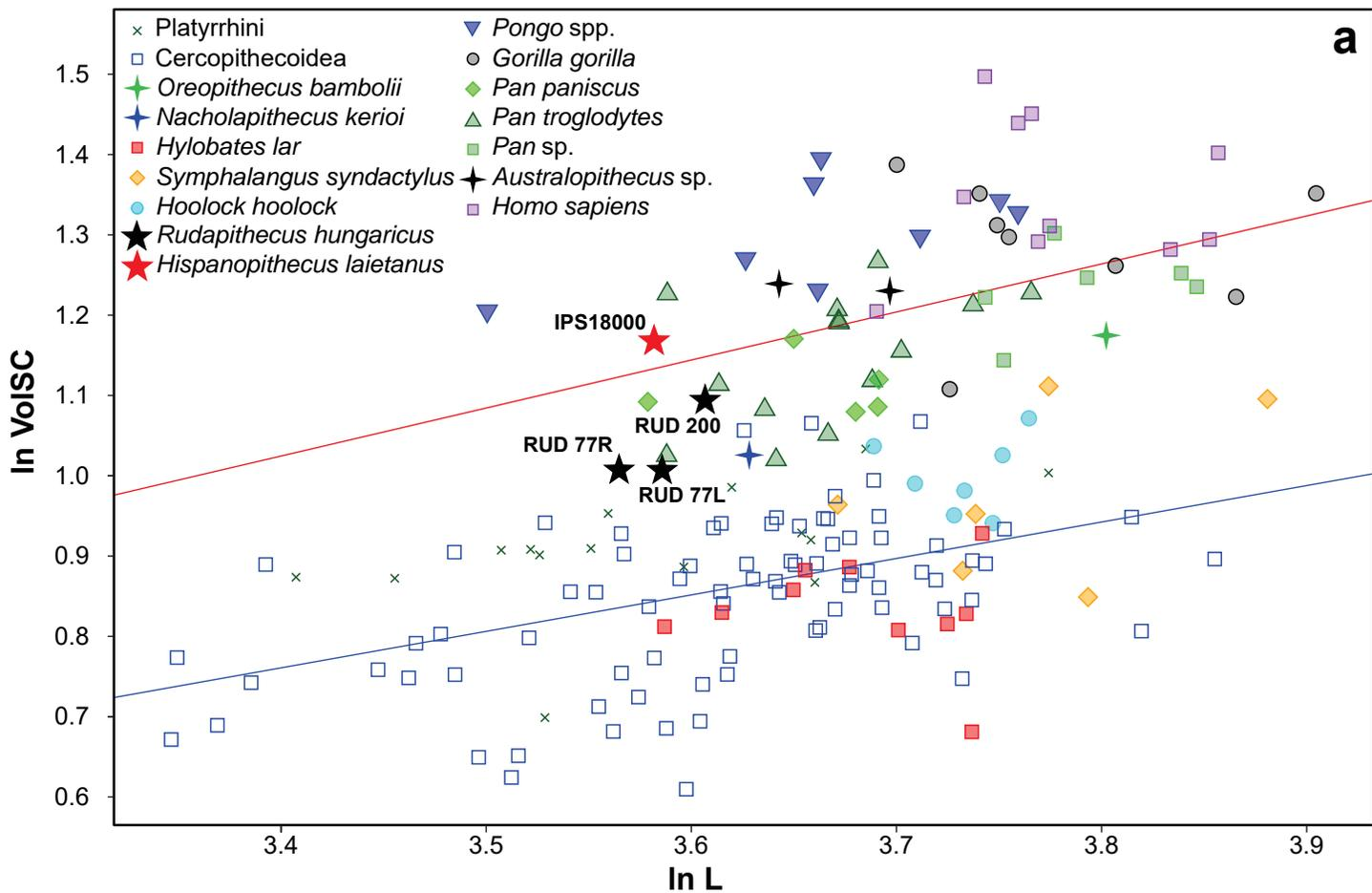


l) *Pan*

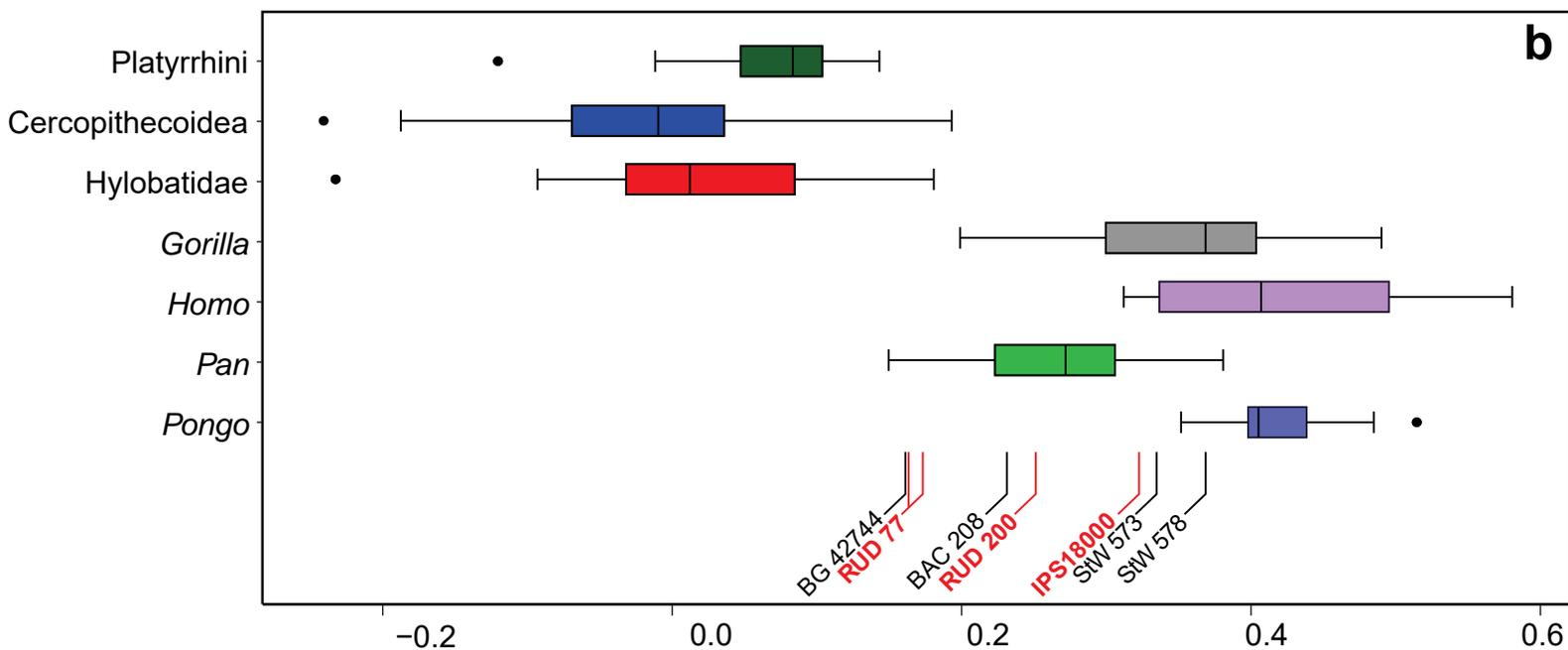


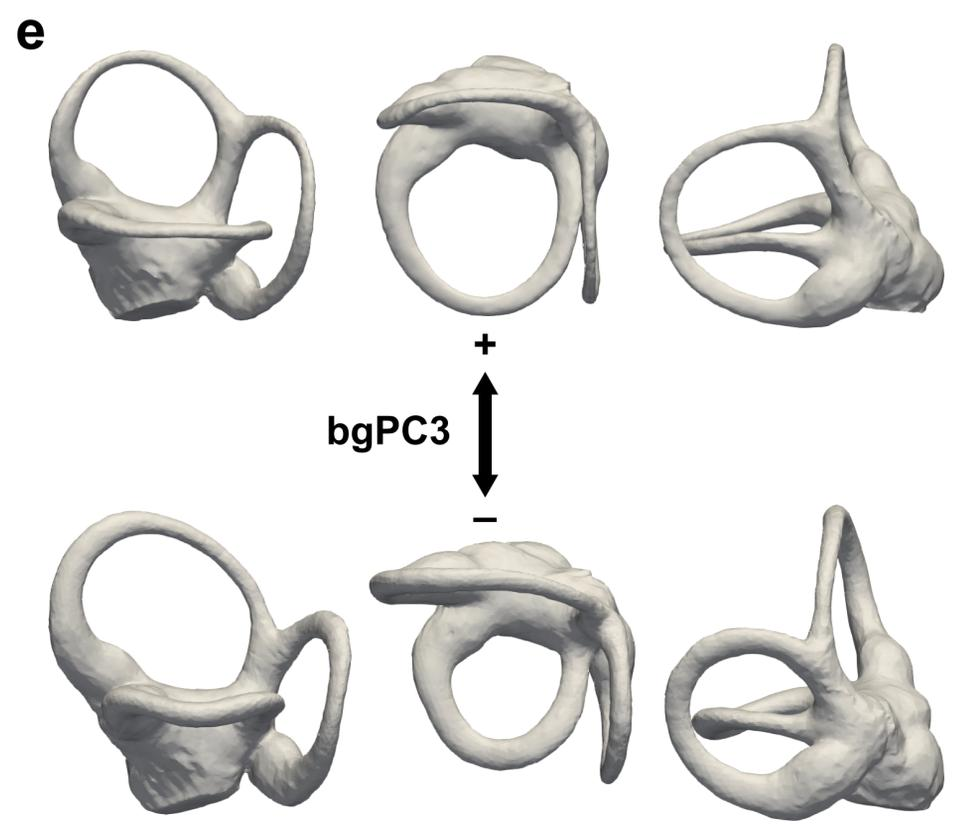
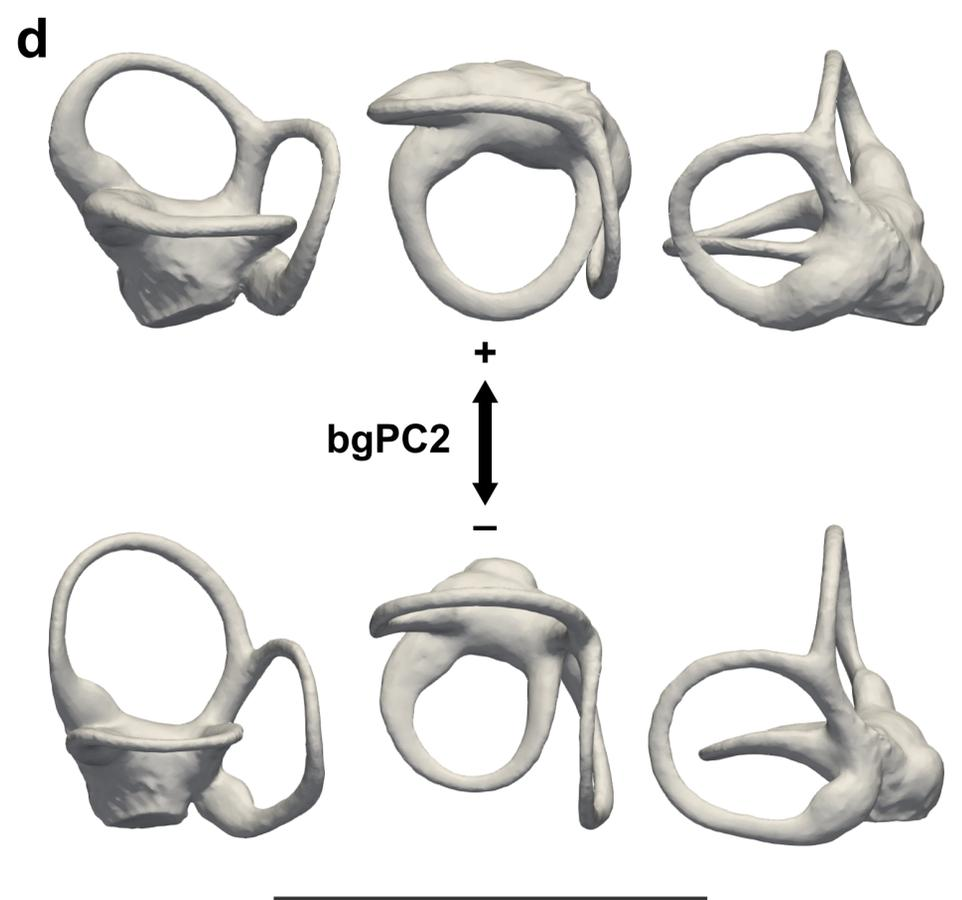
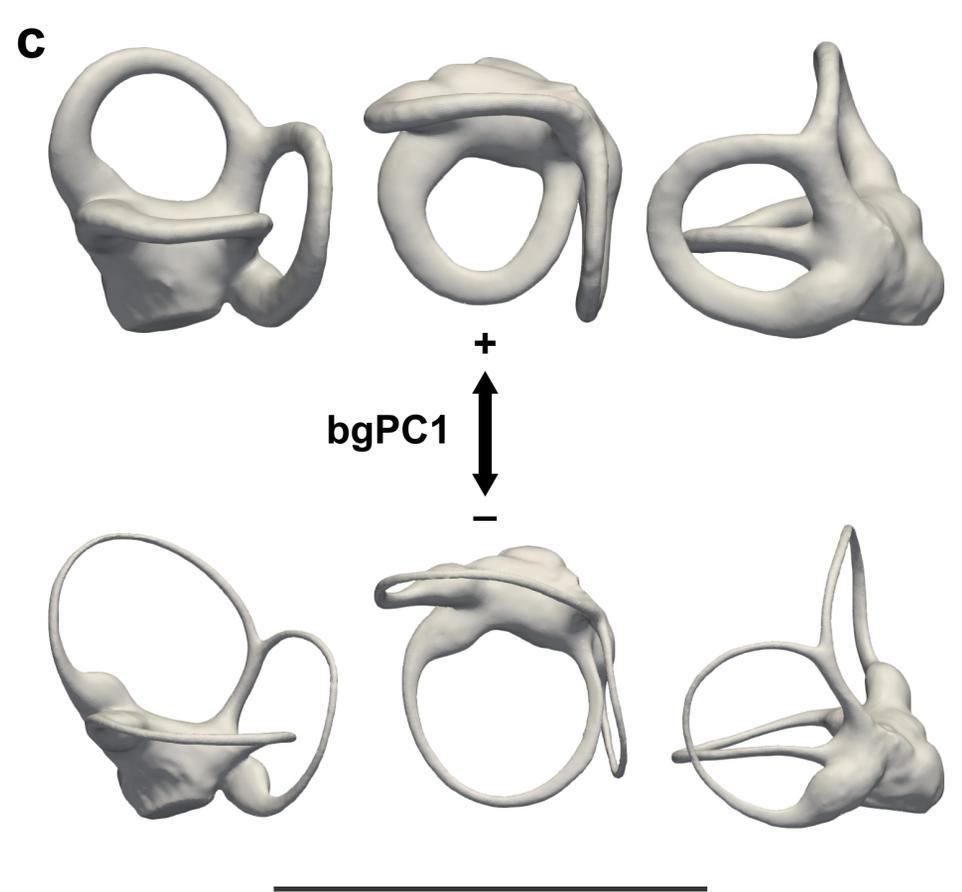
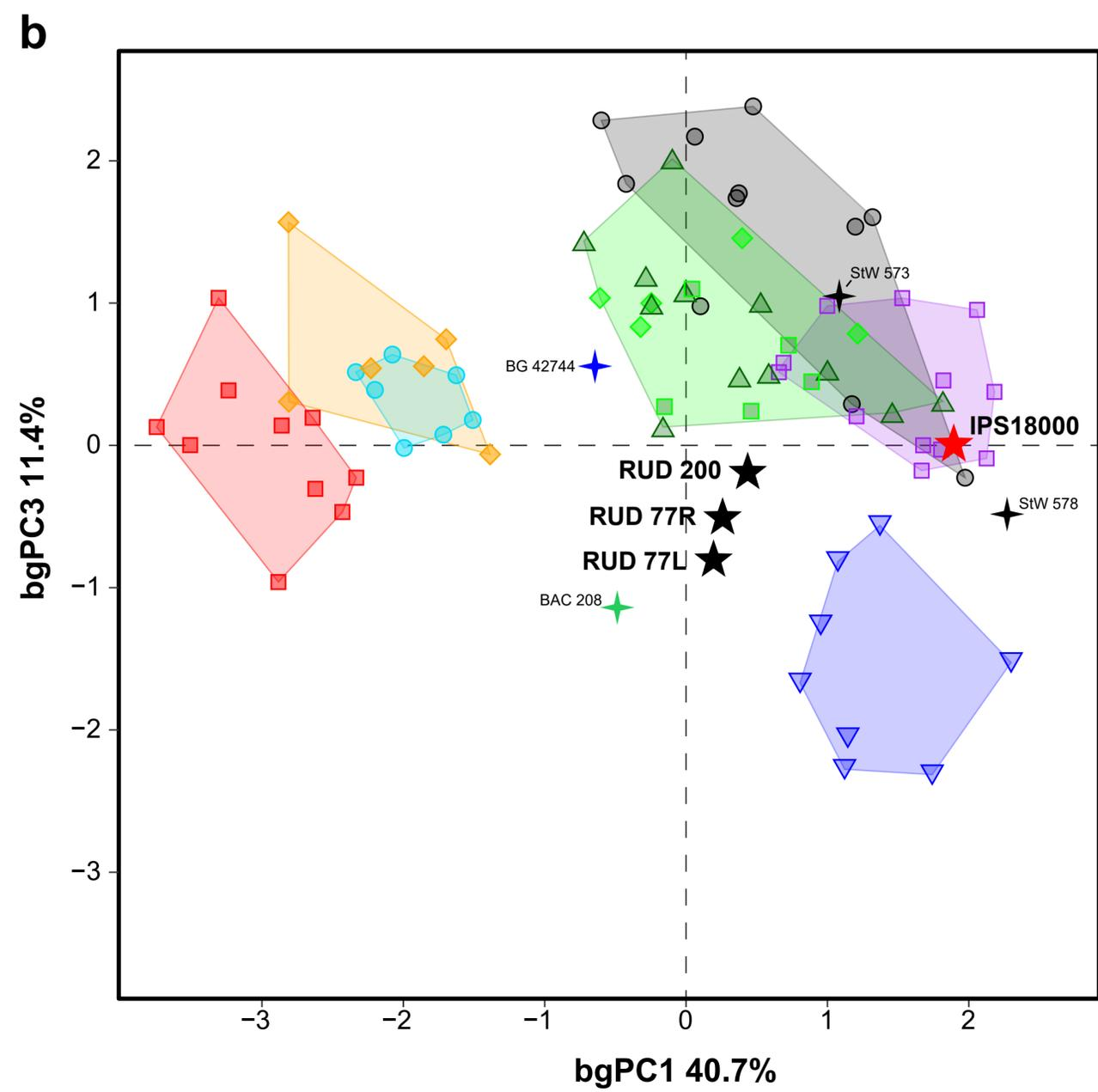
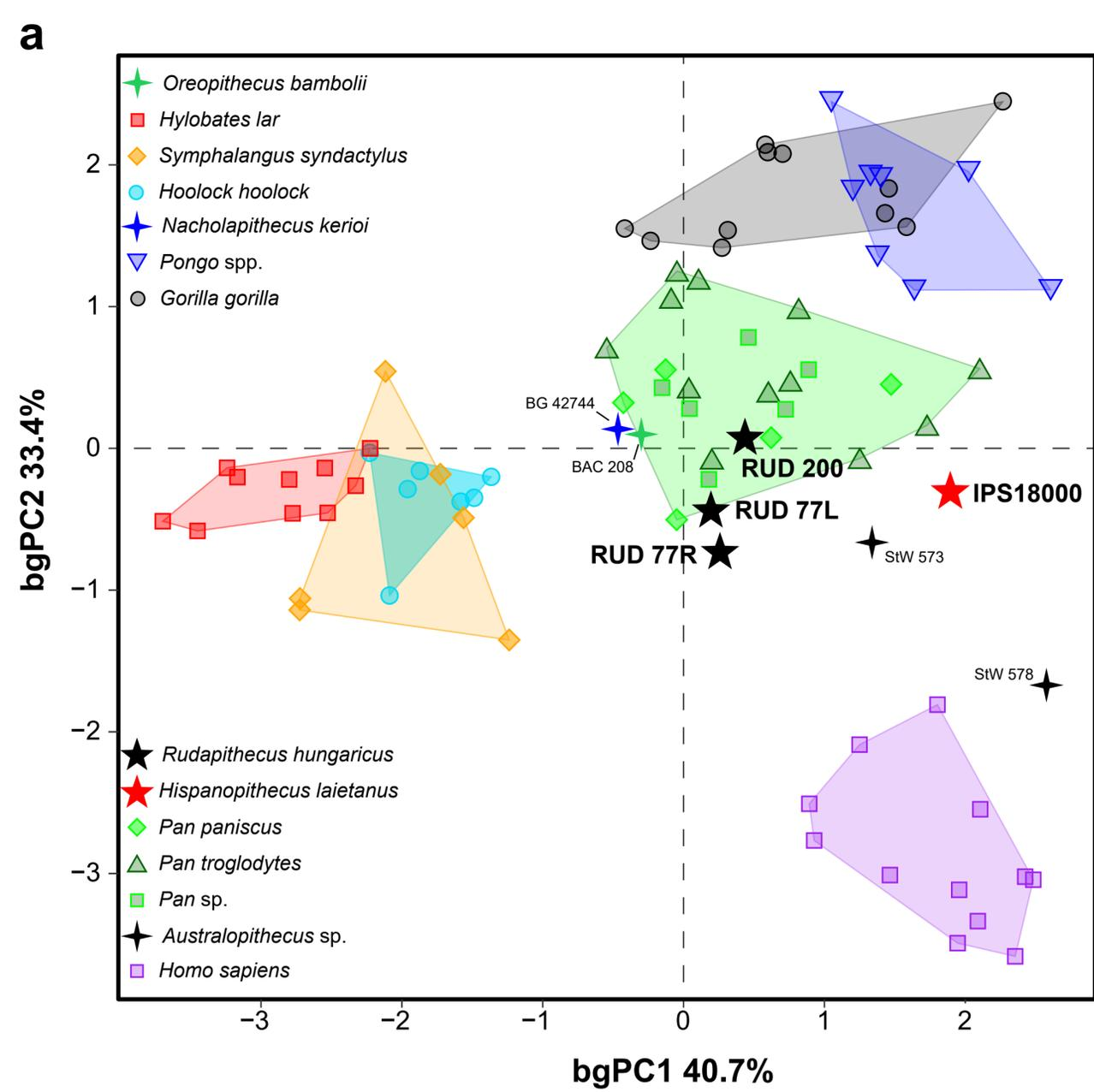
m) *Homo*



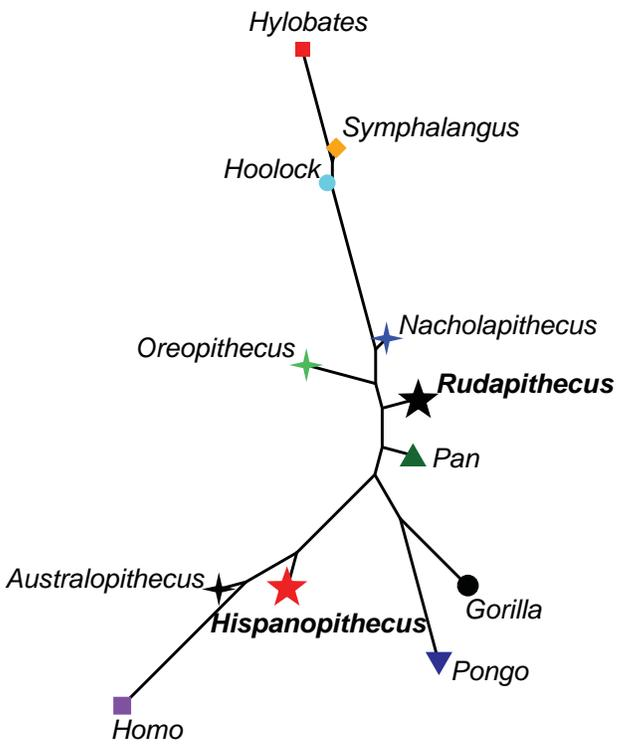


Allometric residuals

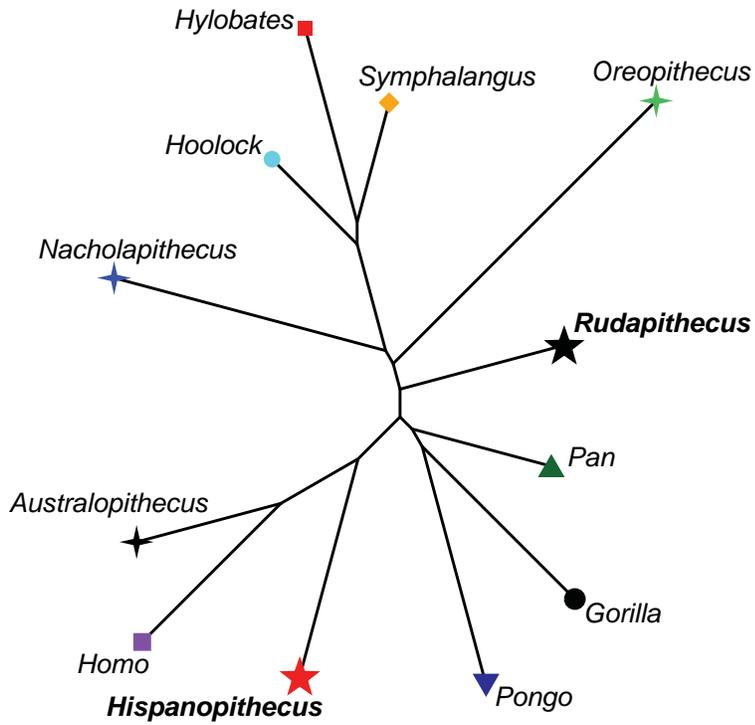


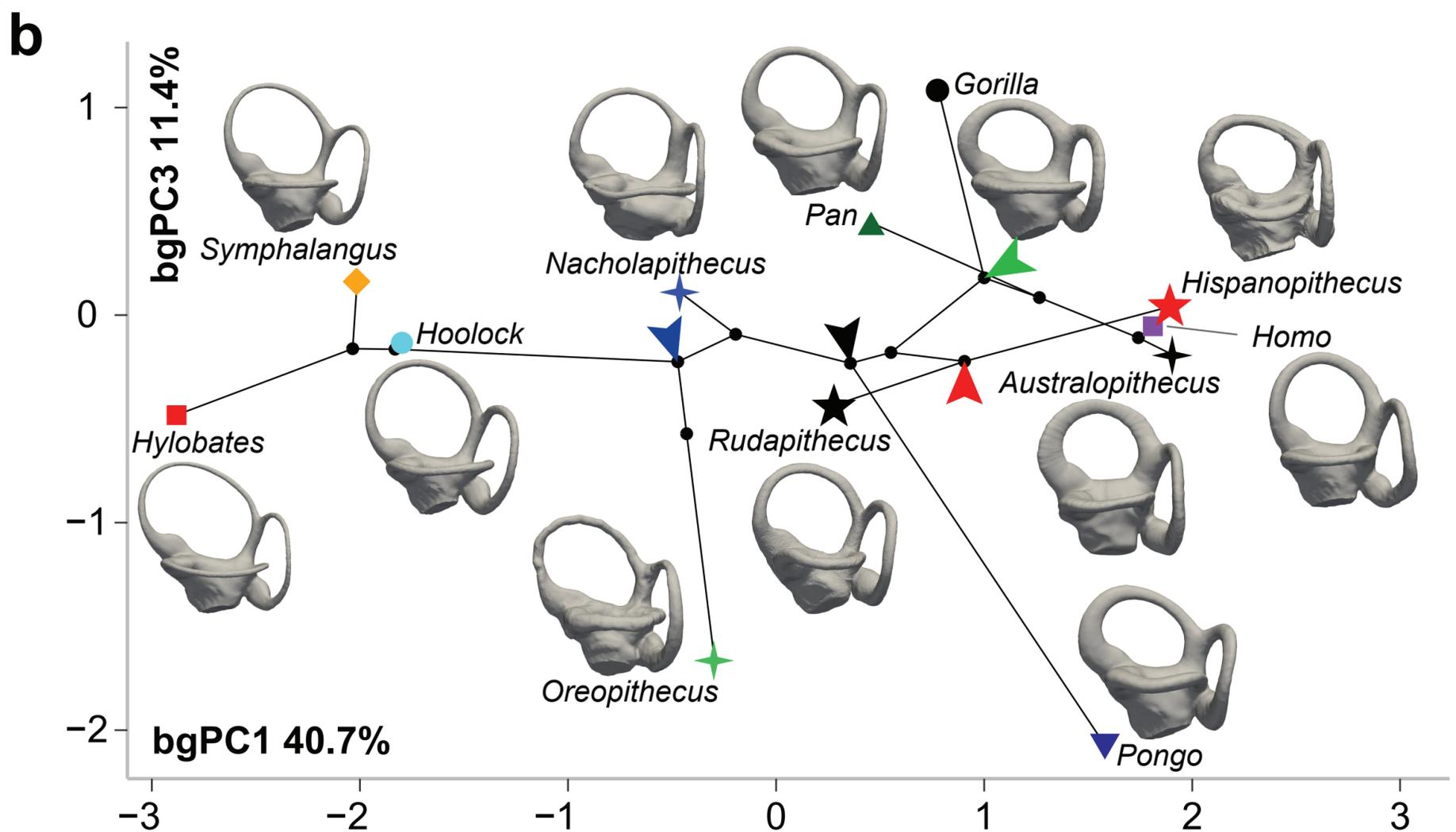
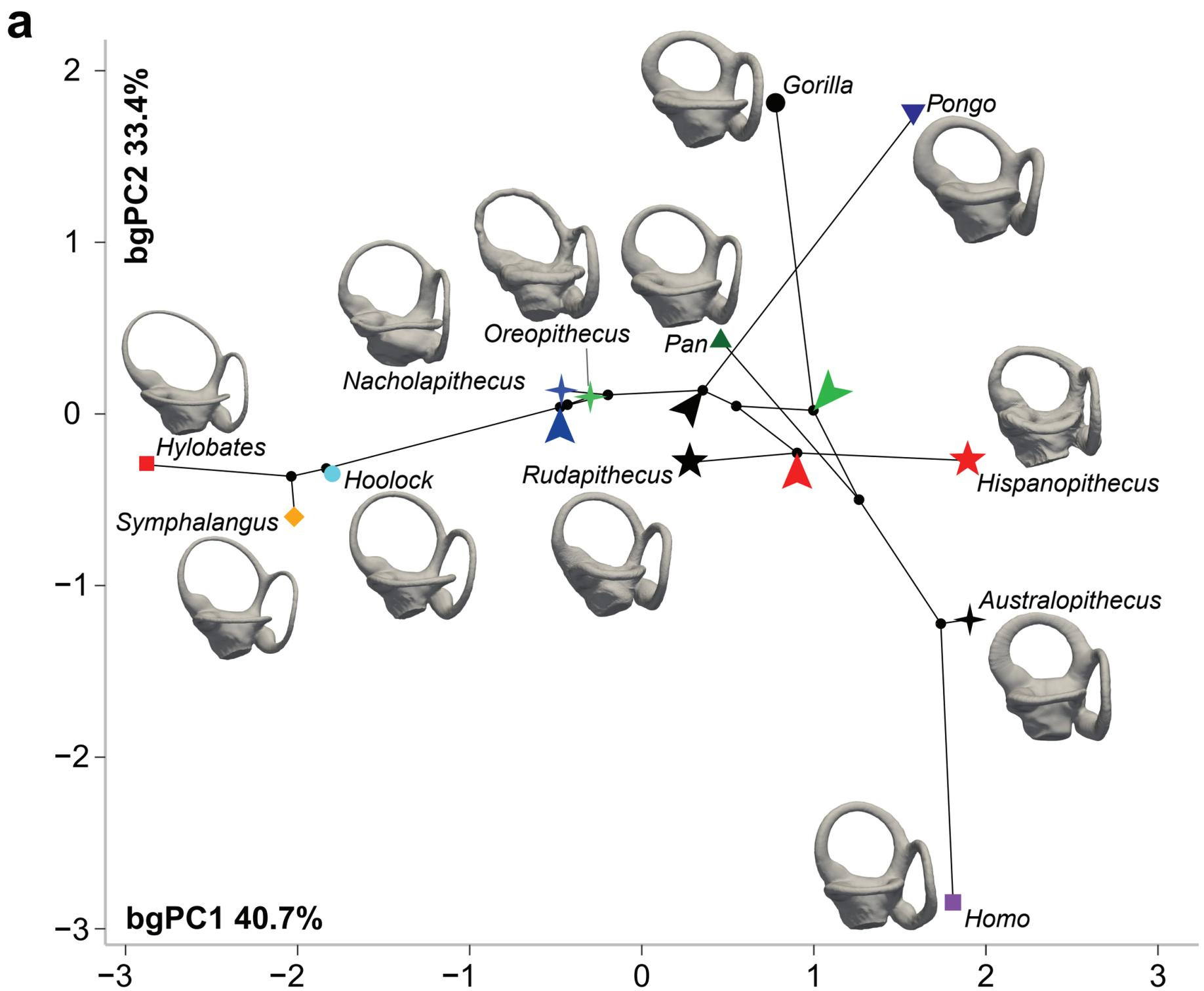


a



b





▶ Crown hominoid LCA
 ▶ Crown hominid LCA
 ▶ Crown hominine LCA
 ▶ Dryopithecine LCA

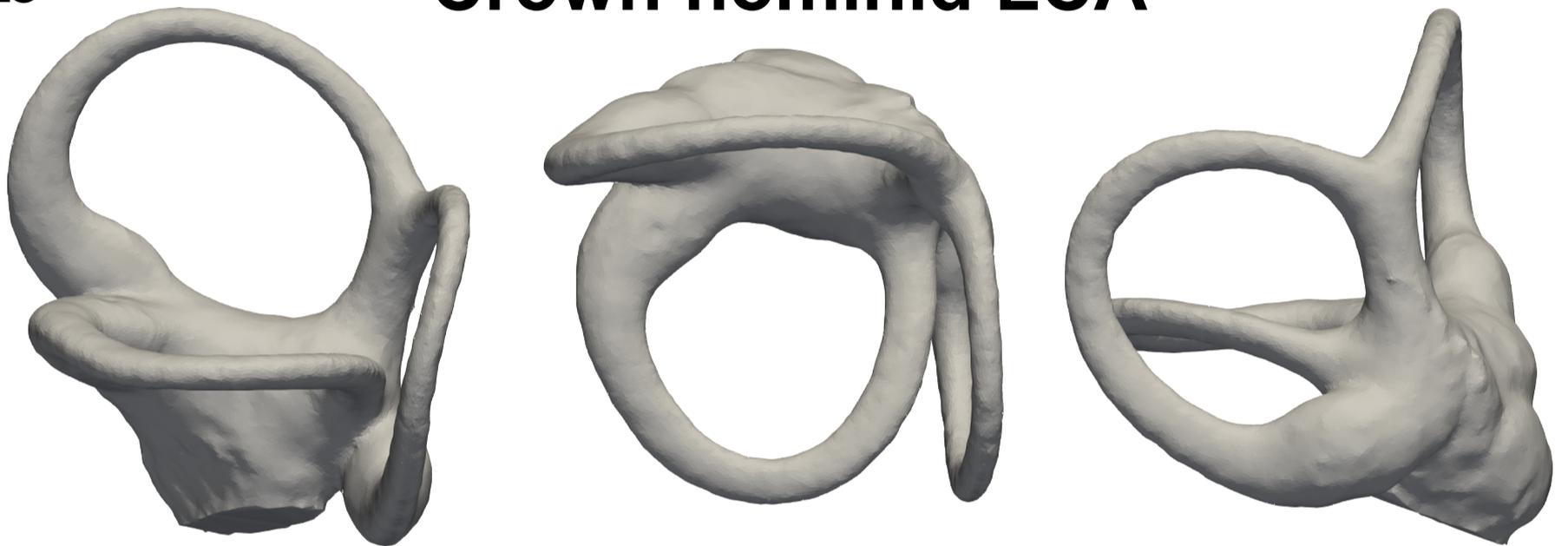
a

Crown hominoid LCA



b

Crown hominid LCA



c

Crown hominine LCA



d

Dryopithecine LCA



- 1 **Table 2 Mahalanobis distances (D^2) between dryopiths and other fossils.** These distances are based on the scores of the
- 2 significant between-group principal components (bgPC1–bgPC3).

D^2	IPS18000	RUD 77R	RUD 77L	RUD 200
IPS18000 (<i>Hispanopithecus laietanus</i>)	—	2.037	2.504	1.012
RUD 77R (<i>Rudapithecus hungaricus</i>)	2.037	—	0.179	0.772
RUD 77L (<i>Rudapithecus hungaricus</i>)	2.504	0.179	—	0.848
RUD 200 (<i>Rudapithecus hungaricus</i>)	1.012	0.772	0.848	—
BAC 208 (<i>Oreopithecus bamboli</i>)	6.678	2.495	1.385	3.571
BG 42744 (<i>Nacholapithecus kerioi</i>)	2.286	1.270	1.505	0.416
StW 573 (<i>Australopithecus</i> sp.)	0.703	2.587	3.657	1.637
StW 578 (<i>Australopithecus</i> sp.)	3.080	2.745	3.087	4.479

- 3
- 4
- 5